

UNIVERSIDAD AUTONOMA DE MADRID

ESCUELA POLITÉCNICA SUPERIOR



TRABAJO FIN DE GRADO

**Análisis y diseño de bocinas con perfiles arbitrarios
mediante análisis modal**

Lucas Polo López

Mayo 2014

Abstract

Horn antennas are widely used in communication systems. They are typically used as feeds for reflector antennas and, due to its robustness, they can also be mounted on the fuselage of airplanes and are used on-board satellites. Horn antennas also present great directivities, gains, and efficiencies. The main drawback of this antenna family is (as it happens with most microwave devices) that they are pretty complicated to simulate with full-wave electromagnetic methods.

Most of the commercial tools at the market for simulating microwave devices (CST Microwave Studio, HFSS,...) use general numerical methods such as finite elements or finite differences in time or frequency domain, whose main advantage is that they can tackle a wide range of problems. The main drawback of these general methods is that this generality makes the simulation inefficient, causing long computation times for some problems in comparison with other more analytical techniques. The goal of this work is to develop a software tool capable of analyzing, simulating and designing horn antennas efficiently based on a numerical method, called Mode-Matching, which is known to be very efficient for this type of problem.

Using this software would not only lead to shorter simulation and design times but would also permit to design horn antennas using low performance computers like notebooks.

Resumen

Las antenas de bocina son ampliamente usadas en los sistemas de comunicación. Típicamente se utilizan como alimentadores de antenas reflectoras y, debido a su robustez, también pueden montarse directamente sobre el fuselaje de aviones y a bordo de satélites. Las bocinas tienen la virtud de presentar grandes valores de directividad, ganancia y eficiencia. La principal desventaja de esta familia de antenas es (como suele ocurrir con la mayoría de los dispositivos de microondas) que son bastante complicadas de simular electromagnéticamente.

La mayoría de las herramientas comerciales existentes en el mercado para la simulación de dispositivos de microondas (CST Microwave Studio, HFSS,...) usan métodos numéricos genéricos como son el de elementos finitos o el de diferencias finitas (bien en el dominio del tiempo o en el de la frecuencia), cuya principal ventaja es que permiten atacar un amplio rango de problemas. La principal desventaja de estos métodos genéricos es precisamente que su generalidad hace la simulación ineficiente, provocando largos tiempos de computación para ciertos problemas en comparación con otras técnicas más analíticas. El objetivo de este trabajo es el de desarrollar una herramienta software capaz de analizar, simular y diseñar antenas de bocina de forma eficiente basada en un método numérico, llamado Análisis Modal, el cual es muy eficiente para este tipo de problemas.

El uso de este software permitirá no sólo reducir los tiempos de simulación y diseño si no también el diseñar antenas de bocina utilizando ordenadores de bajo rendimiento como los notebook.

Keywords/Palabras clave

English

Antenna, beamwidth, circular waveguide, corrugations, directive gain, directivity, discontinuity, evanescent mode, far field, fundamental mode, high order mode, horn, main lobe, microwave, Mode-Matching, propagating mode, radiation pattern, rectangular waveguide, scattering matrix, side lobe, waveguide, waveguide mode

Español

Antena, ancho de haz, guía de onda circular, corrugaciones, ganancia directiva, directividad, discontinuidad, modo evanescente, campo lejano, modo fundamental, modo de orden superior, bocina, lóbulo principal, microondas, Análisis Modal, modo propagante, diagrama de radiación, guía de onda rectangular, matriz de dispersión, lóbulo secundario, guía de onda, modo en guía de onda

Contents

1	Introduction	1
1.1	Motivation	1
1.2	State of the art	2
1.3	Goals	3
1.4	Structure	3
2	Waveguide Simulation	5
2.1	Motivation	5
2.2	Rectangular waveguide	5
2.3	Circular waveguide	6
2.4	Rectangular waveguide resonator	6
2.5	Conclusions	6
3	Mode-Matching method for WG steps	15
3.1	Motivation	15
3.2	Introducing the method	16
3.3	Matching the fields	16
3.4	Computing the Generalized Scattering Matrix	19
3.5	Cascading discontinuities	20
3.6	Study case: H-Plane rectangular waveguide problems	22
	3.6.1 Simulation results of a single step	23
	3.6.2 Two steps with misalignment	24
	3.6.3 Real band-pass filter	24
3.7	Conclusions	30
4	Modeling Horns	33
4.1	Motivation	33
4.2	Stage 1: Inside the horn	33

4.3	Stage 2: Outside the horn	35
4.4	Conclusions	38
5	Verification cases	39
5.1	Motivation	39
5.2	Tercius	39
5.3	Hispasat 1C	41
5.4	Conical Horn	44
5.5	High Performance Feed Horn	50
5.6	Convergence	50
5.7	Conclusions	52
6	Horn-type antenna design	59
6.1	Motivation	59
6.2	Design process	59
6.3	Non-corrugated conical horn	61
6.4	Corrugated horn	65
6.5	Conclusions	66
7	Conclusions	69

List of Figures

1.1	Waveguide extracted from Wikimedia Commons (Author: Vanessa Ezekowitz). Horn antenna extracted from http://www.radiometer-physics.de	2
2.1	TE_{10} at $10GHz$	7
2.2	TM_{11} at $18GHz$	8
2.3	TE_{44} at $71GHz$	9
2.4	TE_{11} at $5.8GHz$	10
2.5	TM_{01} at $5.8GHz$	11
2.6	TE_{33} at $28GHz$	12
2.7	TE_{112} at $10GHz$	13
3.1	Single step representation [4]	17
3.2	Cascading of two steps. a): Schematic representation of two steps. b): GSM of each step GSM. c): Cascaded GSM.	21
3.3	H-Plane waveguide step	22
3.4	Single step. Aligned guides.	24
3.5	Module of the S-parameters for a single step.	25
3.6	Phase of the S-parameters for a single step.	26
3.7	Two steps. Misaligned guides.	27
3.8	Module of the S-parameters for two steps.	28
3.9	Phase of the S-parameters for two steps.	29
3.10	Band-pass filter representation [7].	30
3.11	Comparison between the results obtained by [7] (3.11a) and the results obtained by the mode-matching software (3.11b)	31
4.1	Profile of different horn types.	34
4.3	Horn antenna characterized by its GSM.	35

4.2	Representation of the two methods used to model a smooth horn. Dashed green shows the real profile and solid red the discrete one.	36
5.1	3D representation of Tercius	40
5.2	Tercius radiation pattern. Comparison between Mode-Matching computation and CST Studio Microwave.	42
5.3	Profile of the Hispasat 1C	44
5.4	Hispasat 1C horn radiation pattern. $f = 11.7GHz$. Mode-Matching results (dashed red) of this work are superimposed on the graphs provided by [8].	45
5.5	Hispasat 1C horn radiation pattern. $f = 14GHz$. Mode-Matching results (dashed red) of this work are superimposed on the graphs provided by [8].	46
5.6	Return loses of the Hispasat 1C. Solid red: Reference [6]. Dashed blue: Mode-Matching with 70 modes at the aperture. Dotted black: Mode-Matching with 120 modes at the aperture.	47
5.7	Discretized profile of different horns	48
5.8	Conical Horn simulation (blue, thick) compared with theoretical and measured data from [9] (black, thin). $f = 12.5GHz$	49
5.9	High performance feed horn simulation compared with measurement data by [10].	51
5.10	Convergence of the radiation pattern for different discretization methods.	53
5.11	Convergence of the radiation pattern for different number of modes at the horn aperture.	54
5.12	Convergence of the radiation pattern for different number of waveguide steps.	55
5.13	Convergence study of the return loses.	56
6.1	Horn design flowchart	60
6.2	Radiation pattern of the non-corrugated conical horn at $10GHz$. E-Plane: Solid blue, H-Plane: Dashed green.	62
6.3	Comparison of the results by Mode-Matching (solid) and CST Studio (dashed) at $10GHz$	63
6.4	Return losses of the designed antennas.	64
6.5	Parameters of the corrugation. Extracted from [2].	66

6.6 Radiation pattern of the non-corrugated conical horn at $10GHz$.
E-Plane: Solid blue, H-Plane: Dashed green. 67

List of Tables

3.1	Band-pass filter measurements [7].	27
5.1	Dimensions of the waveguide steps (10 waveguide sections) at Tercius.	41
5.2	Measurements of the High Performance Feed Horn [10].	50

Glossary

- **Antenna:** A device used to radiate or receive electromagnetic waves.
- **Beamwidth:** Angular distance measured on the radiation pattern between points of a given power value.
- **Corrugations:** At a horn antenna. Slots carved at the inner surface of the horn. They produce the effect of having the same radiation pattern at both main planes.
- **Directivity:** Of an antenna. Relation between the power density radiated in the direction of strongest emission versus the power density radiated by an isotropical antenna.
- **Evanescent mode:** A waveguide mode that it is not propagating at the operation frequency. They may appear next to discontinuities or next to the generator but they do not travel far since they become attenuated quickly.
- **Far field:** Electromagnetic region far from the antenna where the radiation pattern does not change with the distance.
- **Fundamental mode:** Of a transmission medium. The mode with the lowest cutoff frequency.
- **GSM:** Stands for Generalized Scattering Matrix. The term *Generalized* refers to the fact that the matrix takes on account not only propagating modes but the evanescent ones too.
- **High order mode:** Of a transmission medium. All the modes that are not the fundamental.

- **Horn:** Antenna composed by a flaring waveguide. They present high directivity values and low losses.
- **Main lobe:** Of a radiation pattern, the lobe with the greatest value.
- **Microwave:** Range of the electromagnetic spectrum from $300MHz$ to $300GHz$.
- **Mode-Matching:** Quasi-analytical waveguide analysis method.
- **Propagating mode:** A waveguide mode that is propagating at the operation frequency.
- **Radiation pattern:** Of an antenna. Representation of how the radiated power varies with the angular direction.
- **Scattering matrix:** Matrix that relates the power waves incident and scattered at the different ports of a device.
- **Side lobe:** Of a radiation pattern. All the lobes that are not the main lobe.
- **TE:** Of a waveguide mode. Stands for “Transverse Electric”, meaning that the electric field does not have a component along the propagation direction.
- **TM:** Of a waveguide mode. Stands for “Transverse Magnetic”, meaning that the magnetic field does not have a component along the propagation direction.
- **Waveguide:** Metallic pipe used as a transmission medium.
- **Waveguide mode:** Each of the solutions of the wave equation inside a waveguide.

Chapter 1

Introduction

1.1 Motivation

Horn antennas are widely used in communication systems [1, 2]. They are, basically, a waveguide (see an example at Figure 1.1a on the following page) [3] whose transverse section increases progressively along its longitudinal axis. Therefore horns (see an example at Figure 1.1b on the next page) share the main advantages that waveguides present. Horn antennas tend to be very robust and, since the dielectric filling them is usually air (or vacuum), these devices present small losses.

These two properties along with the high directivity gain levels achieved by horn antennas make them specially suited for aerospace applications. Horns can be used as a feed for a parabolic reflector antenna or they can be mounted on the fuselage of an airplane or spacecraft.

The main disadvantage of horn antennas (as it happens with most waveguide devices) lies in the analysis procedures for their accurate characterization. Traditionally the approach to model waveguide devices has been based on equivalent circuits using transmission lines and lumped components. Despite these models have permitted to design many devices, they also have some important limitations. The most significant is that they are only focused on modeling the fundamental mode response and the localized effects of higher order modes, but they do not take on account interactions between higher order modes and other complex electromagnetic effects that appear inside a waveguide. These simplifications usually lead to a mismatch between the design and the measured results.

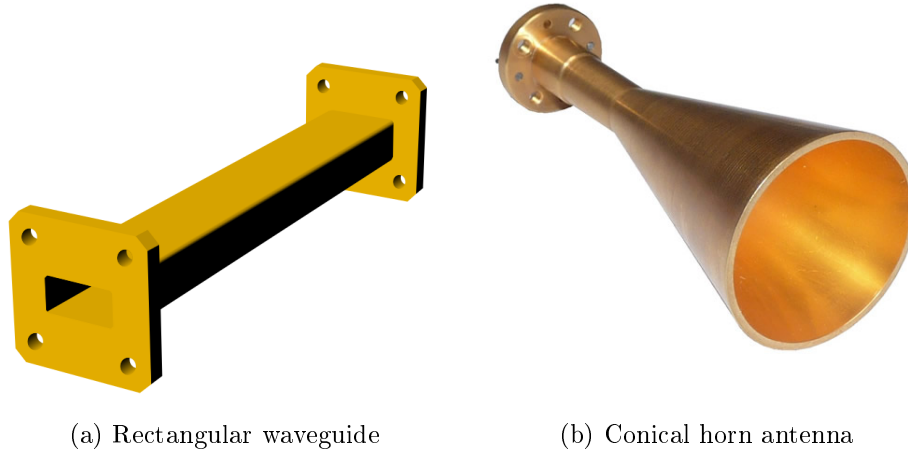


Figure 1.1: Waveguide extracted from Wikimedia Commons (Author: Vanessa Ezekowitz). Horn antenna extracted from <http://www.radiometer-physics.de>.

Fortunately, the development of computers and Computer Aided Design (CAD) tools [4] have provided engineers with the ability to perform more accurate electromagnetic simulations of these devices.

1.2 State of the art

Nowadays the numeric methods implemented by CAD tools classify in two main families, general numeric techniques (like Finite Differences Method and Finite Elements Method) and quasi-analytical techniques (such as the Mode-Matching Method) [4, 1, 2]. General numeric methods are the option habitually chosen for commercial tools and they have a clear advantage over quasi-analytical methods which is their ability to tackle a wide range of problems.

Of course this generality comes at a price and the main disadvantage of general numeric methods is that they are inefficient for some particular problems, giving therefore longer computation times. On the other hand, quasi-analytical methods [4, 5, 6] are usually more efficient but they can just work with a narrow spectrum of problems.

1.3 Goals

The goal of this work is to develop a software tool capable of analyzing, simulating and designing horn antennas efficiently. The key idea is to implement a software as light as possible that can be executed on simple computers like notebooks. In order to fulfill this requisite the chosen method must belong to the quasi-analytical family. It is the Mode-Matching method.

The developed software must allow to design a horn antenna within a short amount of time and then, before constructing it, the design could also be simulated using a commercial tool in order to double-check the validity of the Mode-Matching results. In this design process, the general numeric methods are only used at the end, just for verification, reducing significantly the total design time.

1.4 Structure

To achieve the above described goal the project has been divided in five steps, each one corresponding to a chapter of the present document

1. The understanding of horn antennas requires to work with waveguide modes. Thus, the first step in this project has been to develop a MATLAB based simulator of the electromagnetic fields inside a waveguide.
2. The next step was to study the theory of Mode-Matching, and in order to get a better comprehension of the method, a MATLAB program has been created to simulate waveguide discontinuities.
3. The far-field radiated by a horn can be computed based on the electric field at the horn aperture. This electric field may be obtained using the modal amplitudes provided by a Mode-Matching analysis. In order to perform this analysis the antenna must be first modeled as a succession of waveguide steps.
4. After the development phase we had to test our software. We accomplished this by simulating different antennas from a selection of publications, and measured results coming from actual devices on-board satellites, and checking our results with the ones provided by other authors.

5. Once we were sure that our implementation was working correctly, we have designed a couple of antennas using the developed software. This design step has shown the usefulness of the proposed approach.

Before these five chapters there is the introduction chapter. At the end, there is also a chapter for conclusions and future work.

Chapter 2

Waveguide Simulation

2.1 Motivation

Given the deep theoretical background of this work it seemed a good idea to start developing a simulator which can compute and plot the electromagnetic fields inside a waveguide in order to get a main idea of what is happening in the problem under study. Doing this it would be easier to deal with the mathematical abstractions (mostly scattering parameters).

Two simple guides have been selected (rectangular and circular) and two MATLAB programs have been developed that compute the electric and magnetic fields for every spot inside the defined guide. The program plots a transverse view of the guide at the given longitudinal position.

2.2 Rectangular waveguide

To display the utility of the code, some examples are shown in the following pages. For a waveguide of $19.05mm \times 9.525mm$ (corresponding this dimensions with the normalized guide WR-75) the following pictures depict a vector representation of the electric and magnetic fields and a color-plot of the Poynting vector. The equations implemented in this code (for both the rectangular and circular waveguide) can be found in many sources, such as [3] and will not be repeated here.

- TE_{10} (fundamental mode). Figure 2.1 on page 7.
- TM_{11} (first propagating TM mode). Figure 2.2 on page 8.

- TE_{44} (a higher order mode with relatively high number of spatial variations in the waveguide height and width). Figure 2.3 on page 9.

2.3 Circular waveguide

Similarly to the previous section a depiction of some modes of a circular waveguide with a radius of $20mm$ is shown.

- TE_{11} (fundamental mode). Figure 2.4 on page 10.
- TM_{01} (first propagating TM mode). Figure 2.5 on page 11.
- TE_{33} (a higher order mode with relatively high number of spatial variations in the waveguide height and width). Figure 2.6 on page 12.

2.4 Rectangular waveguide resonator

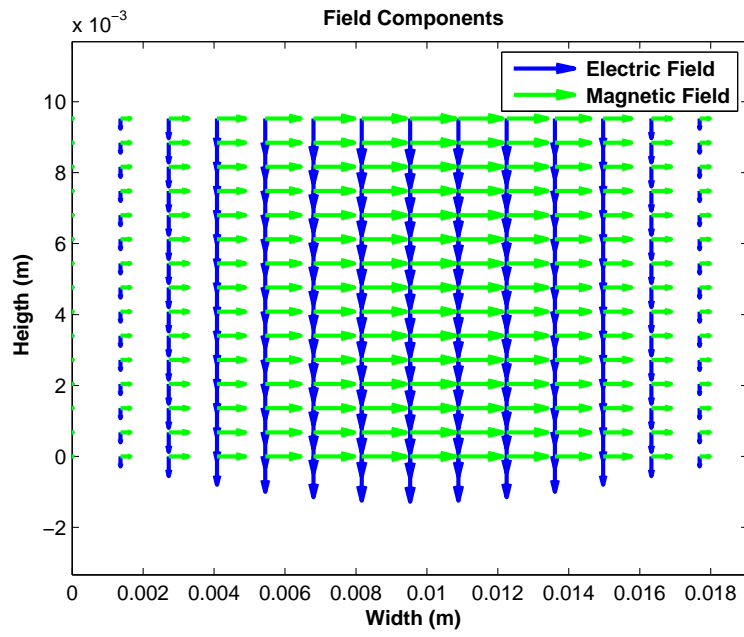
As a last example, the rectangular waveguide code has been modified to represent the electric and magnetic fields of a rectangular waveguide resonant cavity. Different views of the cavity are depicted for the mode TE_{112} resonating at $10GHz$. Figure 2.7 on page 13.

The resonant electromagnetic field is obtained by the superposition of a mode traveling in positive direction and the same mode traveling in negative direction. The expressions of these modes and the resonance frequencies are not displayed here for simplicity. The interested reader may find them at [3].

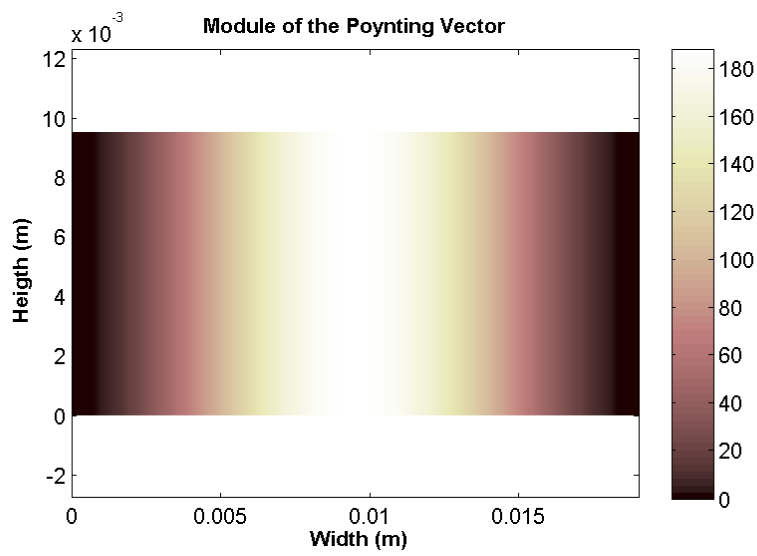
2.5 Conclusions

Developing this simulator has given us some insight on the waveguide modes of a rectangular and circular waveguide. The modes for other waveguides will have different field pattern, but they will be based on the same equations that describe the modes in any closed and metallic waveguide. These expressions have not been included in this work since they can be found in [3]. Furthermore, resonant modes have been also studied. Finally, it is important to say that the circular waveguide will be later used in the horn antennas of this work.

Now we are ready to study the theory of the Mode-Matching method.

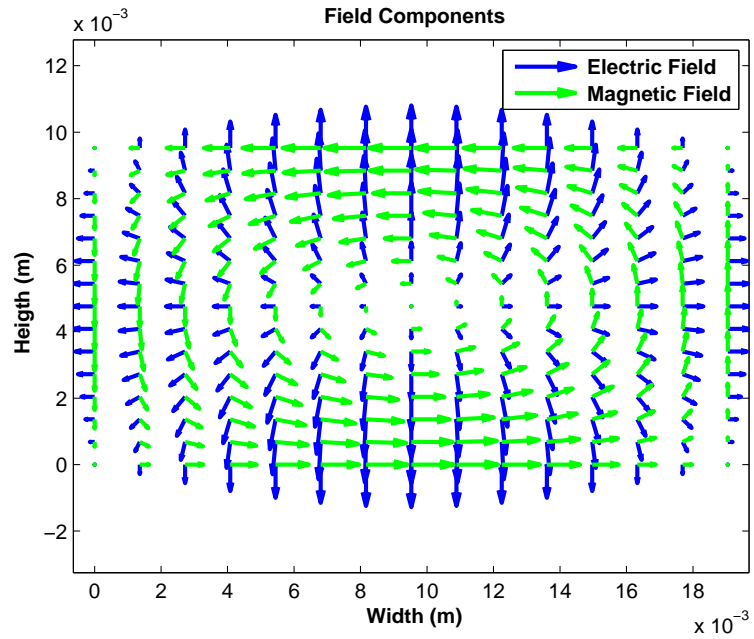


(a) Electric and magnetic fields

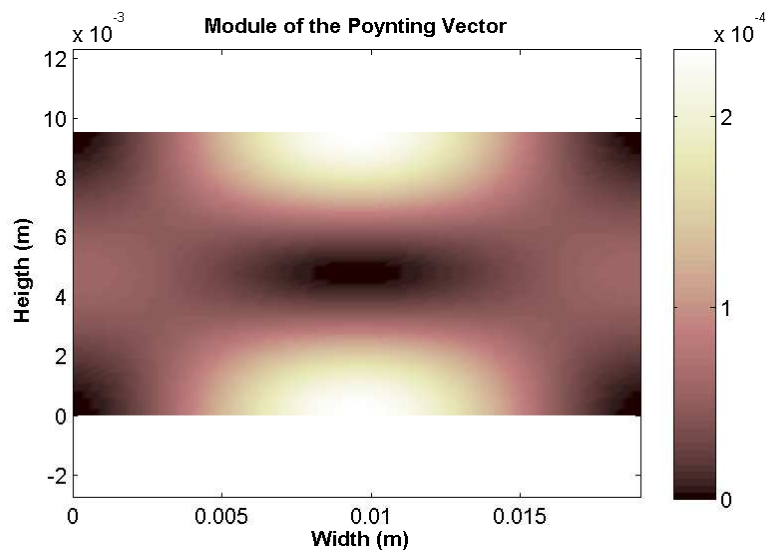


(b) Poynting vector

Figure 2.1: TE_{10} at 10GHz

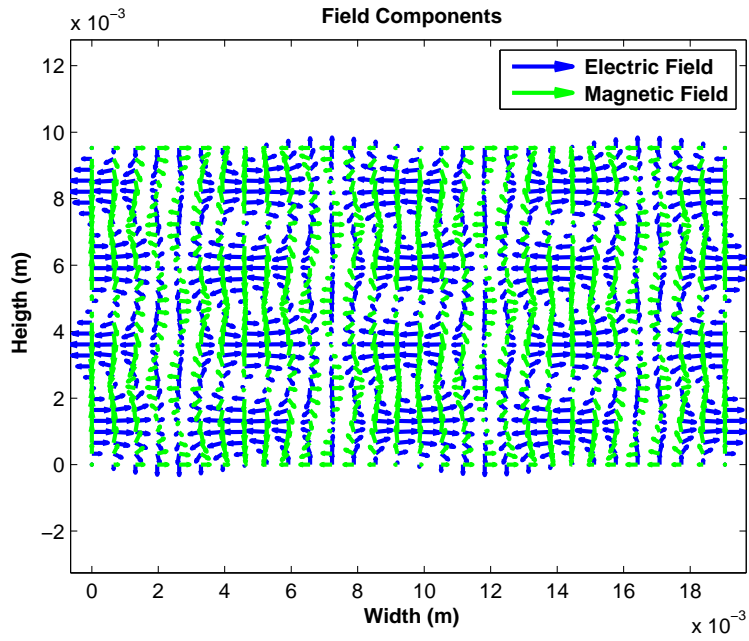


(a) Electric and magnetic fields

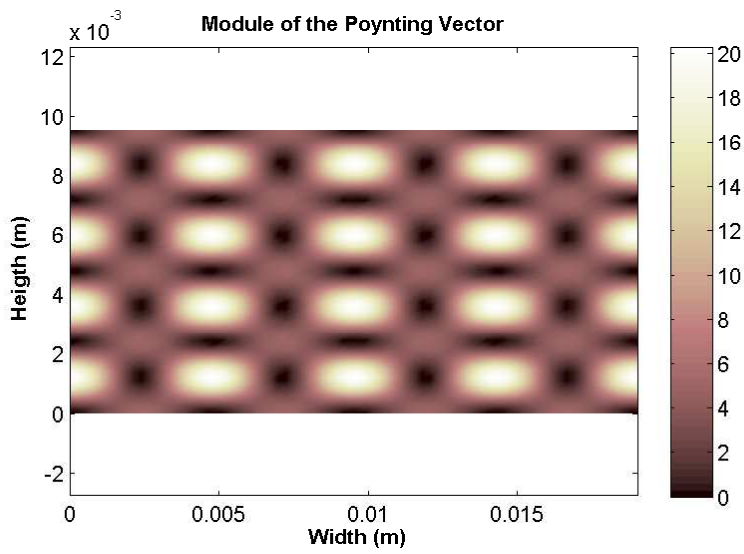


(b) Poynting vector

Figure 2.2: TM_{11} at 18GHz

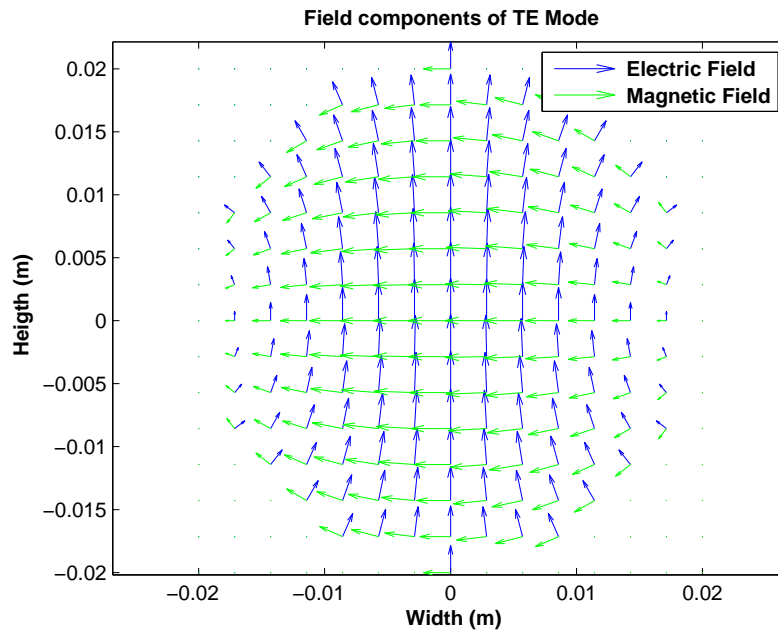


(a) Electric and magnetic fields

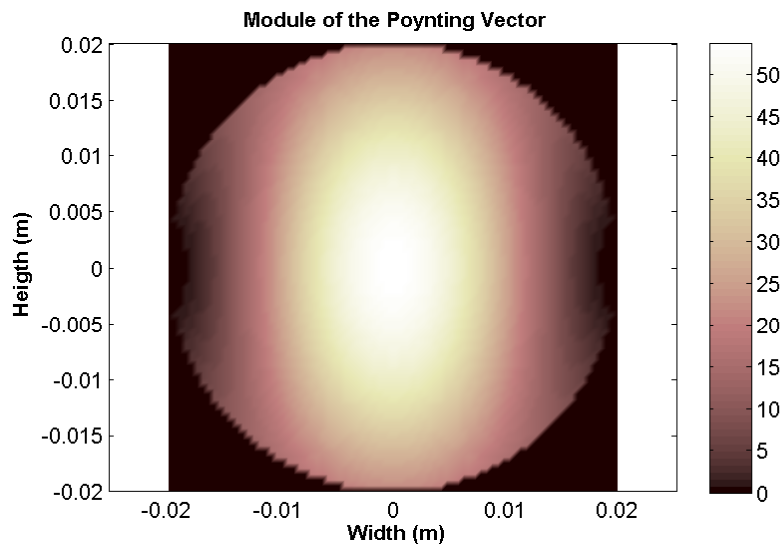


(b) Poynting vector

Figure 2.3: TE_{44} at $71GHz$

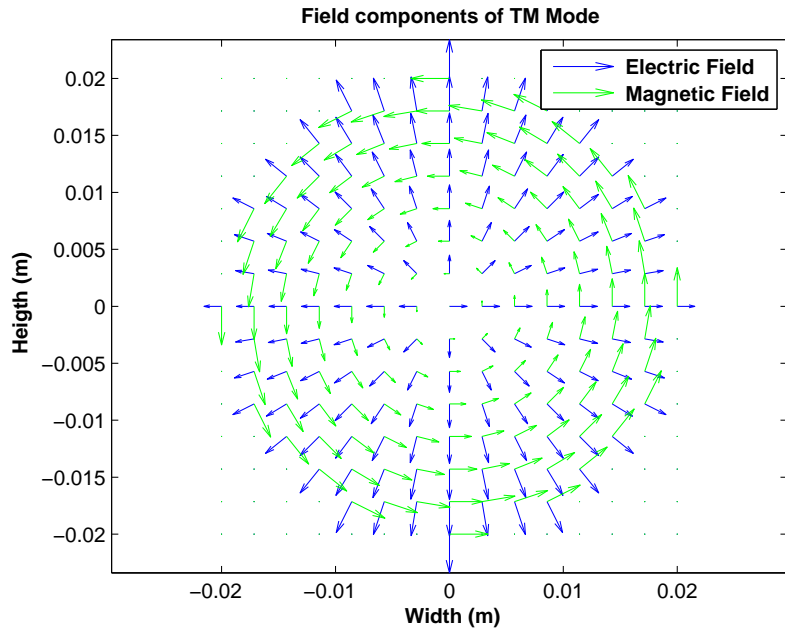


(a) Electric and magnetic fields

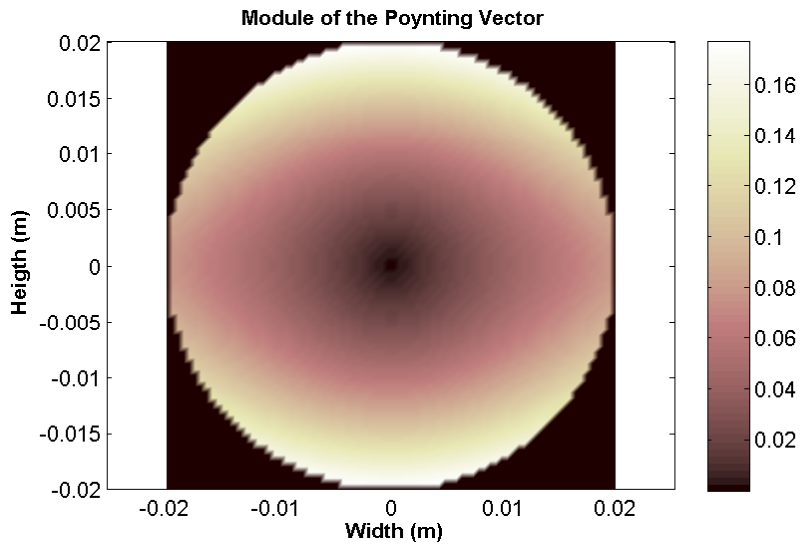


(b) Poynting vector

Figure 2.4: TE_{11} at $5.8GHz$

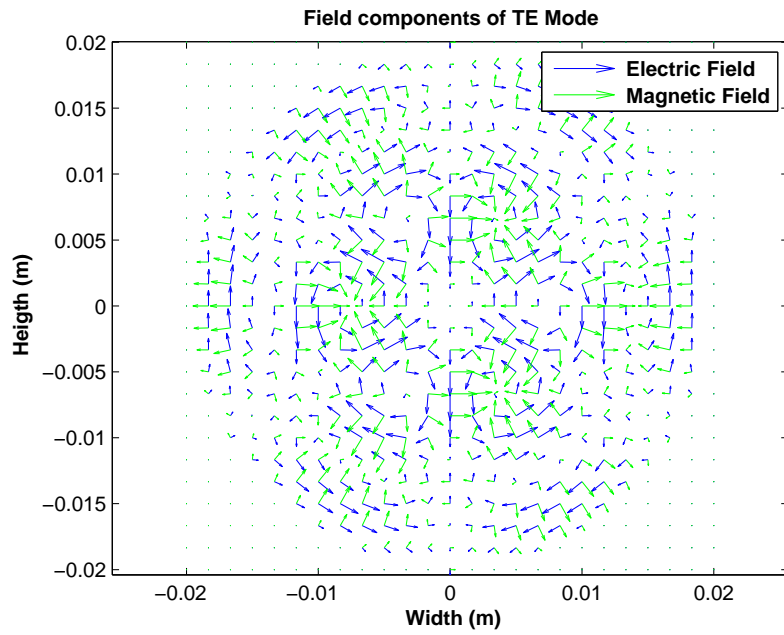


(a) Electric and magnetic fields

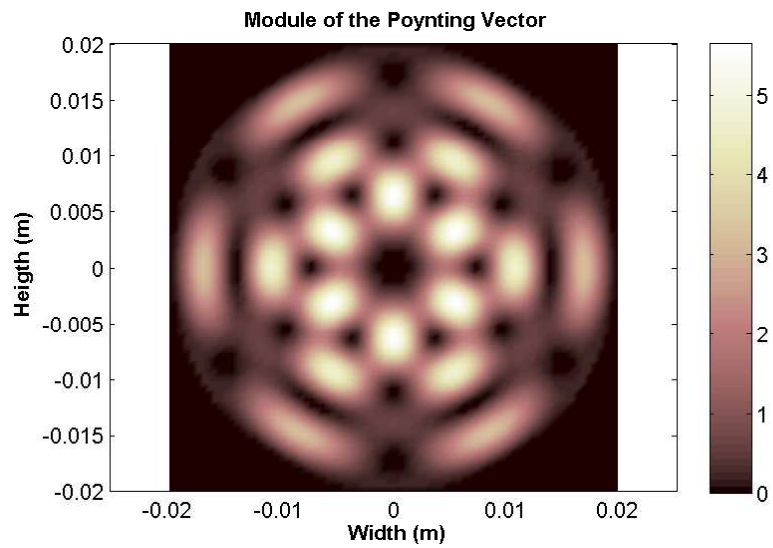


(b) Poynting vector

Figure 2.5: TM_{01} at $5.8GHz$

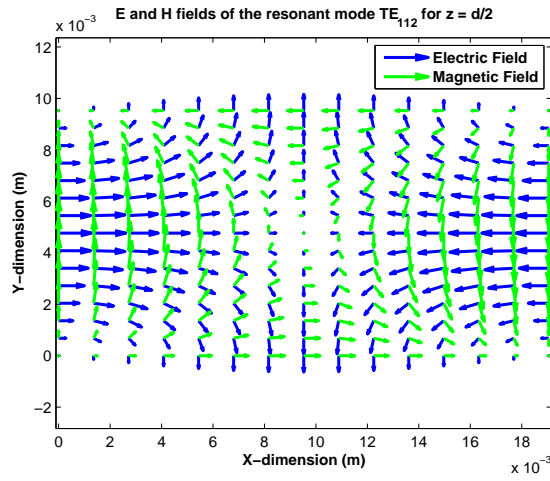


(a) Electric and magnetic fields

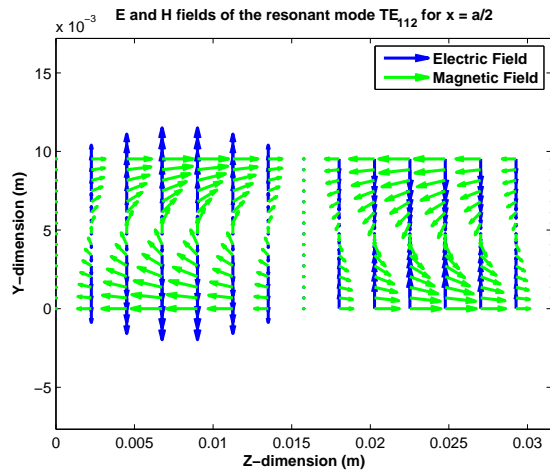


(b) Poynting vector

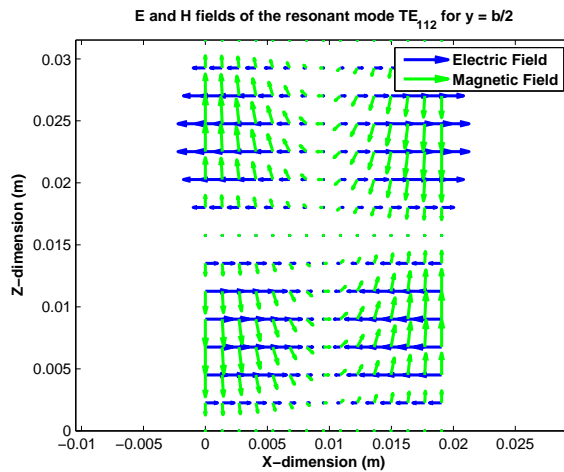
Figure 2.6: TE_{33} at $28GHz$



(a) Frontal view



(b) Lateral view



(c) Upper view

Figure 2.7: TE_{112} at $10GHz$

Chapter 3

Mode-Matching method for WG steps

3.1 Motivation

Traditionally, analysis of waveguide devices has relied on equivalent circuits. These circuits are usually composed of transmission lines (modeling waveguide regions) and lumped components (modeling dissipative effects and discontinuities on the waveguide). However, this kind of modeling has a lot of limitations. The most significant one is that they just model the fundamental mode response and some concrete effects of higher order modes, but they do not take into account interaction between higher order modes and other complex electromagnetic effects that appear inside a waveguide.

This simplification, in the spite of being useful for an initial design of a device, or a simplified analysis, usually leads to mismatch between design and measurement results.

With the development of computers in the recent years, CAD (Computer Aided Design) tools have become really useful since they implement complex mathematical methods that can provide a more accurate modeling of the problem. These methods usually classify in generic numeric methods (like the Finite Elements Method and the Finite Differences Method) and quasi-analytic methods. Mode-Matching belongs to this second family and in the rest of this chapter the fundamentals of these mathematical method will be explained.

3.2 Introducing the method

First of all the problem under analysis must be segmented in regions. In each of these regions the electromagnetic field can be represented by the superposition of modes [4, 3]:

$$\vec{\mathbf{E}} = \sum_n \varsigma_n^+ \vec{\mathbf{E}}_n^+ + \sum_n \varsigma_n^- \vec{\mathbf{E}}_n^-, \quad \vec{\mathbf{H}} = \sum_n \varsigma_n^+ \vec{\mathbf{H}}_n^+ + \sum_n \varsigma_n^- \vec{\mathbf{H}}_n^- \quad (3.1)$$

The complex amplitudes (ς_n^\pm) may initially be undetermined, and the electromagnetic modal field ($\vec{\mathbf{E}}_n^\pm, \vec{\mathbf{H}}_n^\pm$) must be known in advance (either analytically or numerically). This modal expansion provides a formal solution to Maxwell equations, but in order to get a complete solution the boundary conditions must be satisfied at the interfaces between different regions.

In order to make computations easier, modal amplitudes from each region are usually organized into vectors which are related by the GSM (Generalized Scattering Matrix) [4]. The objective throughout the whole process would be to compute this GSM.

Although the modal expansion defines a complete representation of the electromagnetic field, in order to implement the Mode-Matching method on a real computer, the summations at (3.1) must be truncated so then convergence problems may arise. These problems would depend not only on the number of modes taken on account but also on the relation between the number of modes considered at each side of the discontinuity.

3.3 Matching the fields

In this chapter are only developed the equations for a particular case in order to avoid getting lost with the algebra so it is only considered the situation where one section of the guide is completely included inside the other guide section ($A_s \subseteq A_w$, see Figure 3.1 on the next page). More complex cases can be analyzed on a similar way [4].

Modal amplitudes at both sides of the discontinuity can be derived from the modal expansion. The boundary conditions must be fulfilled by field component transverse to z evaluated at $z = 0^\pm$. The fields at this point are expressed in function of the modes incident and scattered.

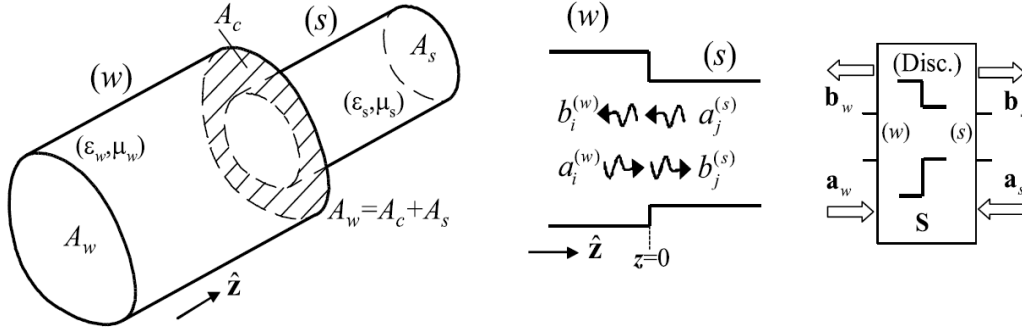


Figure 3.1: Single step representation [4]

$$(3.2) \quad \vec{\mathbf{E}}_t^{(w)} \Big|_{A_w, z=0^-} = \sum_{n=1}^{N_w} (a_n^{(w)} + b_n^{(w)}) \vec{\mathbf{e}}_n^{(w)}, \quad \vec{\mathbf{H}}_t^{(w)} \Big|_{A_w, z=0^-} = \sum_{n=1}^{N_w} (a_n^{(w)} - b_n^{(w)}) \vec{\mathbf{h}}_n^{(w)}$$

$$\vec{\mathbf{E}}_t^{(s)} \Big|_{A_s, z=0^+} = \sum_{m=1}^{N_s} (b_m^{(s)} + a_m^{(s)}) \vec{\mathbf{e}}_m^{(s)}, \quad \vec{\mathbf{H}}_t^{(s)} \Big|_{A_s, z=0^+} = \sum_{m=1}^{N_s} (b_m^{(s)} - a_m^{(s)}) \vec{\mathbf{h}}_m^{(s)} \quad (3.3)$$

It should be observed that now the series are truncated to the number of modes taken at each region. Each term of the expansion corresponds with a TEM, TE or TM mode (not necessarily propagating at the operation frequency). It is also important to note that these modes are orthogonal with arbitrary normalization:

$$\iint_{A_g} \vec{\mathbf{e}}_n^{(g)} \times \vec{\mathbf{h}}_m^{(g)} \cdot \hat{\mathbf{z}} dS = Q_n^{(g)} \delta_{nm}, \quad g \equiv w, s, \quad \delta_{nm} = \begin{cases} 1 & m = n \\ 0 & m \neq n \end{cases} \quad (3.4)$$

The boundary conditions are:

$$\begin{cases} EFBC \text{ in } A_w : \hat{\mathbf{z}} \times \vec{\mathbf{E}}^{(w)} = \begin{cases} 0 & \text{in } A_c, z = 0 \\ \hat{\mathbf{z}} \times \vec{\mathbf{E}}^{(s)} & \text{in } A_s, z = 0 \end{cases} \\ MFBC \text{ in } A_s : \hat{\mathbf{z}} \times \vec{\mathbf{H}}^{(w)} = \hat{\mathbf{z}} \times \vec{\mathbf{H}}^{(s)} \text{ in } A_s, z = 0 \end{cases} \quad (3.5)$$

Where EFBC stands for “Electric Field Boundary Conditions” and MFBC for “Magnetic Field Boundary Conditions”. These conditions must be satisfied at both sides of the discontinuity.

First, EFBC is tested with a generic modal magnetic field $\vec{\mathbf{h}}_j^{(w)}$ of waveguide (w):

$$\iint_{A_w} (\hat{\mathbf{z}} \times \vec{\mathbf{E}}^{(w)}) \cdot \vec{\mathbf{h}}_j^{(w)} dS = \sum_{n=1}^{N_w} (a_n^{(w)} + b_n^{(w)}) \left(\iint_{A_w} (\hat{\mathbf{z}} \times \vec{\mathbf{e}}^{(w)}) \cdot \vec{\mathbf{h}}_j^{(w)} dS \right) \quad (3.6)$$

Where (3.2) has been used at the left hand side. Taking into account that the modes are orthogonal (see (3.4)) the equation simplifies to:

$$\iint_{A_w} (\hat{\mathbf{z}} \times \vec{\mathbf{E}}^{(w)}) \cdot \vec{\mathbf{h}}_j^{(w)} dS = \sum_{n=1}^{N_w} (a_j^{(w)} + b_j^{(w)}) Q_j^{(w)} \quad (3.7)$$

Since $A_w = A_s \cup A_c$ the integration can be divided like:

$$\begin{aligned} \iint_{A_w} (\hat{\mathbf{z}} \times \vec{\mathbf{E}}^{(w)}) \cdot \vec{\mathbf{h}}_j^{(w)} dS &= \\ &= \iint_{A_c} (\hat{\mathbf{z}} \times \vec{\mathbf{E}}^{(w)}) \cdot \vec{\mathbf{h}}_j^{(w)} dS + \iint_{A_s} (\hat{\mathbf{z}} \times \vec{\mathbf{E}}^{(w)}) \cdot \vec{\mathbf{h}}_j^{(w)} dS \end{aligned} \quad (3.8)$$

and given that $\hat{\mathbf{z}} \times \vec{\mathbf{E}}^{(w)} = 0$ in A_c , $z = 0$ and using (3.3) in the integration over A_s it is obtained:

$$\begin{aligned} \iint_{A_w} (\hat{\mathbf{z}} \times \vec{\mathbf{E}}^{(w)}) \cdot \vec{\mathbf{h}}_j^{(w)} dS &= \iint_{A_s} (\hat{\mathbf{z}} \times \vec{\mathbf{E}}^{(w)}) \cdot \vec{\mathbf{h}}_j^{(w)} dS = \\ &= \sum_{m=1}^{N_s} (b_m^{(s)} + a_m^{(s)}) \left\{ \iint_{A_s} \vec{\mathbf{e}}_m^{(s)} \times \vec{\mathbf{h}}_j^{(w)} \cdot \hat{\mathbf{z}} dS \right\} \end{aligned} \quad (3.9)$$

The integral with the modals fields is a complex number usually referred as the inner cross product X_{mj} . Equating (3.7) and (3.9):

$$Q_j^{(w)} (a_j^{(w)} + b_j^{(w)}) = \sum_{m=1}^{N_s} X_{mj} (b_m^{(s)} + a_m^{(s)}), \quad j = 1, \dots, N_w \quad (3.10)$$

Now similar steps can be followed for testing the MFBC. Using the electric fields of waveguide (s):

$$\iint_{A_s} (\hat{\mathbf{z}} \times \vec{\mathbf{H}}^{(w)}) \cdot \vec{\mathbf{e}}_i^{(s)} dS = \sum_{n=1}^{N_w} (a_n^{(w)} - b_n^{(w)}) \left\{ \iint_{A_w} \vec{\mathbf{e}}_i^{(s)} \times \vec{\mathbf{h}}_n^{(w)} \cdot \hat{\mathbf{z}} dS \right\} \quad (3.11)$$

$$\iint_{A_s} (\hat{\mathbf{z}} \times \vec{\mathbf{H}}^{(w)}) \cdot \vec{\mathbf{e}}_i^{(s)} dS = \iint_{A_s} (\hat{\mathbf{z}} \times \vec{\mathbf{H}}^{(s)}) \cdot \vec{\mathbf{e}}_i^{(s)} dS = Q_i^{(s)} (b_i^{(s)} - a_i^{(s)}) \quad (3.12)$$

$$\sum_{n=1}^{N_w} X_{in} (a_n^{(w)} - b_n^{(w)}) = Q_i^{(s)} (b_i^{(s)} - a_i^{(s)}), \quad i = 1, \dots, N_s \quad (3.13)$$

Equations (3.10) and (3.13) may be represented in vector notation.

$$\mathbf{a}_g = [\dots a_n^{(g)} \dots]_{n=1, \dots, N_g}^t, \quad \mathbf{b}_g = [\dots b_n^{(g)} \dots]_{n=1, \dots, N_g}^t, \quad g \equiv w, s \quad (3.14)$$

The normalization constants are collected in the diagonal matrices:

$$\mathbf{Q}_g = \text{diag} [Q_n^{(g)}]_{n=1, \dots, N_g}, \quad g \equiv w, s, \quad [N_g \times N_g] \quad (3.15)$$

and the inner cross product:

$$[X_{mn}] = \iint_{A_s} \vec{\mathbf{e}}_m^{(s)} \times \vec{\mathbf{h}}_n^{(w)} \cdot \hat{\mathbf{z}} dS \quad (3.16)$$

Getting finally the following linear system:

$$\begin{cases} EFBC : & \mathbf{Q}_w (\mathbf{a}_w + \mathbf{b}_w) = \mathbf{X}^t (\mathbf{a}_s + \mathbf{b}_s) \quad (N_w \text{ eqs.}) \\ MFBC : & \mathbf{X} (\mathbf{a}_w - \mathbf{b}_w) = \mathbf{Q}_s (\mathbf{b}_s - \mathbf{a}_s) \quad (N_s \text{ eqs.}) \end{cases} \quad (3.17)$$

3.4 Computing the Generalized Scattering Matrix

The GSM representation of the waveguide step relates the values of \mathbf{b}_w , \mathbf{b}_s (scattered waves) to the values of \mathbf{a}_w , \mathbf{a}_s (incident waves). This relation is expressed as:

$$\begin{bmatrix} \mathbf{b}_w \\ \mathbf{b}_s \end{bmatrix} = \begin{bmatrix} \mathbf{S}_{ww} & \mathbf{S}_{ws} \\ \mathbf{S}_{sw} & \mathbf{S}_{ss} \end{bmatrix} \begin{bmatrix} \mathbf{a}_w \\ \mathbf{a}_s \end{bmatrix}, \quad \mathbf{b} = \mathbf{S}\mathbf{a} \quad (3.18)$$

Each of the terms in the GSM can be computed from (3.17):

$$\mathbf{S} = \begin{bmatrix} \mathbf{Q}_w^{-1}\mathbf{X}^t\mathbf{F}\mathbf{X} - \mathbf{I}_w & \mathbf{Q}_w^{-1}\mathbf{X}^t\mathbf{F}\mathbf{Q}_s \\ \mathbf{F}\mathbf{X} & \mathbf{F}\mathbf{Q}_s - \mathbf{I}_s \end{bmatrix}, \quad \mathbf{F} = 2(\mathbf{Q}_s + \mathbf{X}\mathbf{Q}_w^{-1}\mathbf{X}^t)^{-1}, \quad (3.19)$$

where \mathbf{I}_g is the identity matrix of size N_g .

So in summary, the process for obtaining the GSM of a waveguide step is the following:

1. Select the number of modes taken into account at each waveguide section ($\mathbf{N}_w, \mathbf{N}_s$).
2. Fill the normalization matrices ($\mathbf{Q}_w, \mathbf{Q}_s$).
3. Fill the inner cross product matrix (\mathbf{X}) (3.16).
4. Compute the GSM (3.19).

Whether the method converges or not depends not just on the particular values of $\mathbf{N}_w, \mathbf{N}_s$ but on the relation between these two numbers. This is known as the relative convergence problem. If the proportion is not appropriate the results may not converge even when increasing the number of modes. An usually good point to start is with a relation equal to the ratio between the guides section.

3.5 Cascading discontinuities

The characterization of just one step is not of much use when dealing with a real world problem. Fortunately the procedures exposed above can also be used when working with complex structures. The key idea is to divide the device under study in different steps, compute the GSM of each one of these steps and then compute the GSM of the whole structure by cascading the partial GSMs. This process is depicted at Figure 3.2 on the facing page.

In order to develop some intuition around this topic it will be considered the characterization of a waveguide with two discontinuities. Each of the

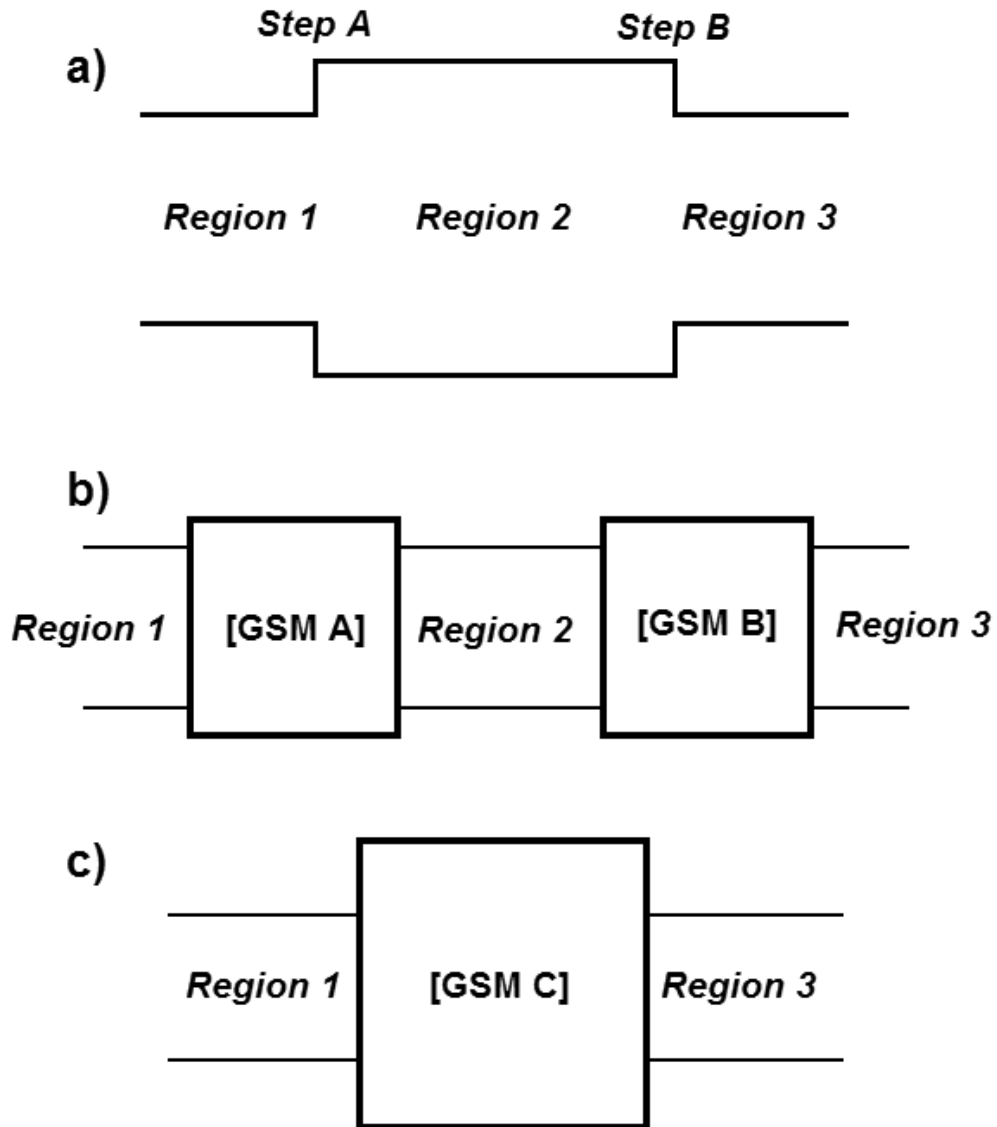


Figure 3.2: Cascading of two steps. a): Schematic representation of two steps. b): GSM of each step. c): Cascaded GSM.

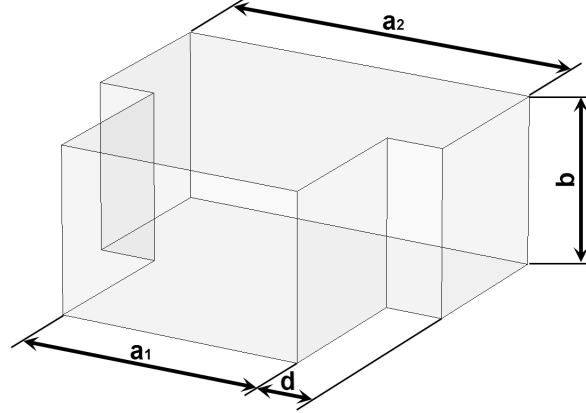


Figure 3.3: H-Plane waveguide step

steps can be pictured as a block (called block A and block B) of which its GSM is known: $\mathbf{b}^{(A)} = \mathbf{S}^{(A)}\mathbf{a}^{(A)}$, $\mathbf{b}^{(B)} = \mathbf{S}^{(B)}\mathbf{a}^{(B)}$. These two blocks are connected by a waveguide of length l , where N_{AB} modes are considered. It is known that on this section of waveguide the modal amplitudes vary with $e^{-\gamma n l}$ so the amplitudes at that region are related by:

$$\mathbf{a}_1^{(B)} = \mathbf{G}\mathbf{b}_2^{(A)}, \quad \mathbf{a}_2^{(A)} = \mathbf{G}\mathbf{b}_1^{(B)}, \quad \mathbf{G} = \text{diag}[e^{-\gamma l}]_{n=1, \dots, N_{AB}} \quad (3.20)$$

And now compute:

$$\mathbf{S}^{(C)} = \begin{bmatrix} \mathbf{S}_{11}^{(A)} + \mathbf{S}_{12}^{(A)}\mathbf{G}\mathbf{H}\mathbf{S}_{11}^{(B)}\mathbf{G}\mathbf{S}_{21}^{(A)} & \mathbf{S}_{12}^{(A)}\mathbf{G}\mathbf{H}\mathbf{S}_{12}^{(B)} \\ \mathbf{S}_{21}^{(B)}\mathbf{G}(\mathbf{I}_{AB} + \mathbf{S}_{22}^{(A)}\mathbf{G}\mathbf{H}\mathbf{S}_{11}^{(B)}\mathbf{G})\mathbf{S}_{21}^{(A)} & \mathbf{S}_{22}^{(B)} + \mathbf{S}_{21}^{(B)}\mathbf{G}\mathbf{S}_{22}^{(A)}\mathbf{G}\mathbf{H}\mathbf{S}_{12}^{(B)} \end{bmatrix},$$

$$\mathbf{H} = (\mathbf{I}_{AB} - \mathbf{S}_{11}^{(B)}\mathbf{G}\mathbf{S}_{22}^{(A)}\mathbf{G})^{-1}, \quad [N_{AB}, N_{AB}] \quad (3.21)$$

Repeating this process iteratively the GSM representing the whole device can be obtained.

3.6 Study case: H-Plane rectangular waveguide problems

At the moment the Mode-Matching method for a generic structure has been formulated. In this section the formulas are particularized for a concrete

3.6. STUDY CASE: H-PLANE RECTANGULAR WAVEGUIDE PROBLEMS23

simple case in order to illustrate the method. A depiction of the problem under study can be found at Figure 3.3 on the preceding page.

Using the well-known results for the rectangular waveguide developed in [3] together with (3.4) and (3.16) the following expressions can be found:

$$X(m_1, m_2) = -Y_m^I \frac{(\omega\mu\pi)^2}{a_1 a_2} \frac{m_1 m_2}{k_{c1}^2 k_{c2}^2} b \int_0^{a_2} \sin\left(\frac{m_1 \pi x}{a_1} + \frac{m_1 \pi (a_1 - a_2)}{2a_1}\right) \sin\left(\frac{m_2 \pi x}{a_2}\right) dx \quad (3.22)$$

$$Q_{m_1}^{(w)} = \frac{\gamma_{m_1}^w (m_1 \pi)^2 b}{j2\omega\mu a_1}, \quad Q_{m_2}^{(s)} = \frac{\gamma_{m_2}^s (m_2 \pi)^2 b}{j2\omega\mu a_2}, \quad (3.23)$$

where $A_w = a_1 \cdot b$ and $A_s = a_2 \cdot b$, and m_j represents the index of the mode taken on account at each waveguide section where $1 \rightarrow w$, $2 \rightarrow s$.

With the idea of getting a deeper comprehension of the Mode-Matching techniques a MATLAB implementation has been developed for the previous study case. In this section some of the results obtained with this program are shown, compared with the results obtained by the commercial software CST Microwave Studio.

3.6.1 Simulation results of a single step

A simple start example is shown in Figure 3.4 on the following page. It shows a single waveguide step with the following dimensions ($d = \frac{a_2 - a_1}{2}$):

Parameter	Value (mm)
a_1	15
a_2	19.05
b	9.525

In this table a refers to the horizontal dimension, b to the vertical dimension and the subscript refers to the waveguide segment.

The simulations are performed for the monomode band so the S-parameters that are represented are the associated with the propagating mode. The representation really corresponds with a subset of the GSM called the “propagating matrix”. This matrix is what is usually referred as the S-parameters of a device [4].

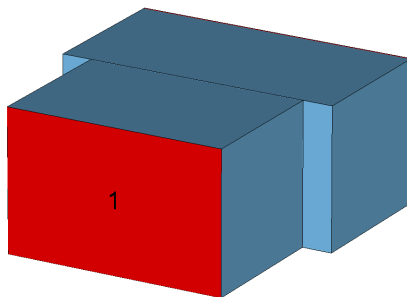


Figure 3.4: Single step. Aligned guides.

It can be appreciated that the results obtained with the MATLAB implementation (Figures 3.5 on the next page and 3.6 on page 26) are pretty the same as the results from CST, but using much less resources. Indeed the Mode-Matching computation of the phase (since the module matches exactly) may be more accurate since a specific ad-hoc method has been used. Calculation times are also much smaller with the MATLAB code.

3.6.2 Two steps with misalignment

Now a more complex case is presented. In Figure 3.7 on page 27 a waveguide structure with two steps is represented. The MATLAB program must compute the GSM for each of these steps and then compute the global GSM by means of (3.21). It is also important to note that now the different waveguide segments are not centrally but laterally aligned, what will lead to a lower transmission parameter. The dimensions of this new structure are ($d_1 = a_2 - a_1$ and $d_2 = a_3 - a_2$):

Parameter	Value (mm)
a_1	15
a_2	19.05
a_3	15
b	9.525

3.6.3 Real band-pass filter

Finally a real filter is simulated in order to demonstrate the practical uses of the developed software. The following design has been extracted from [7]:

3.6. STUDY CASE: H-PLANE RECTANGULAR WAVEGUIDE PROBLEMS25

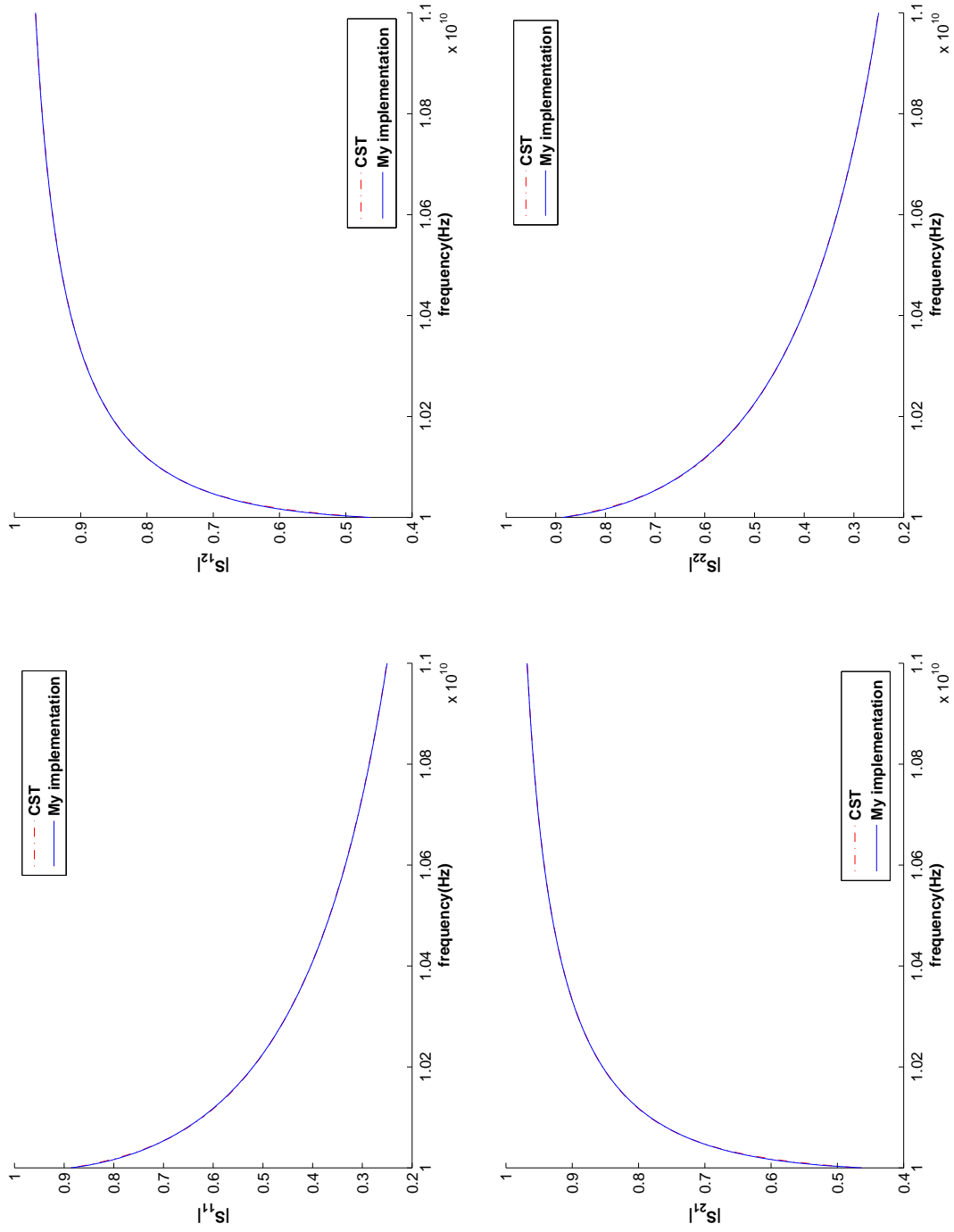


Figure 3.5: Module of the S-parameters for a single step.

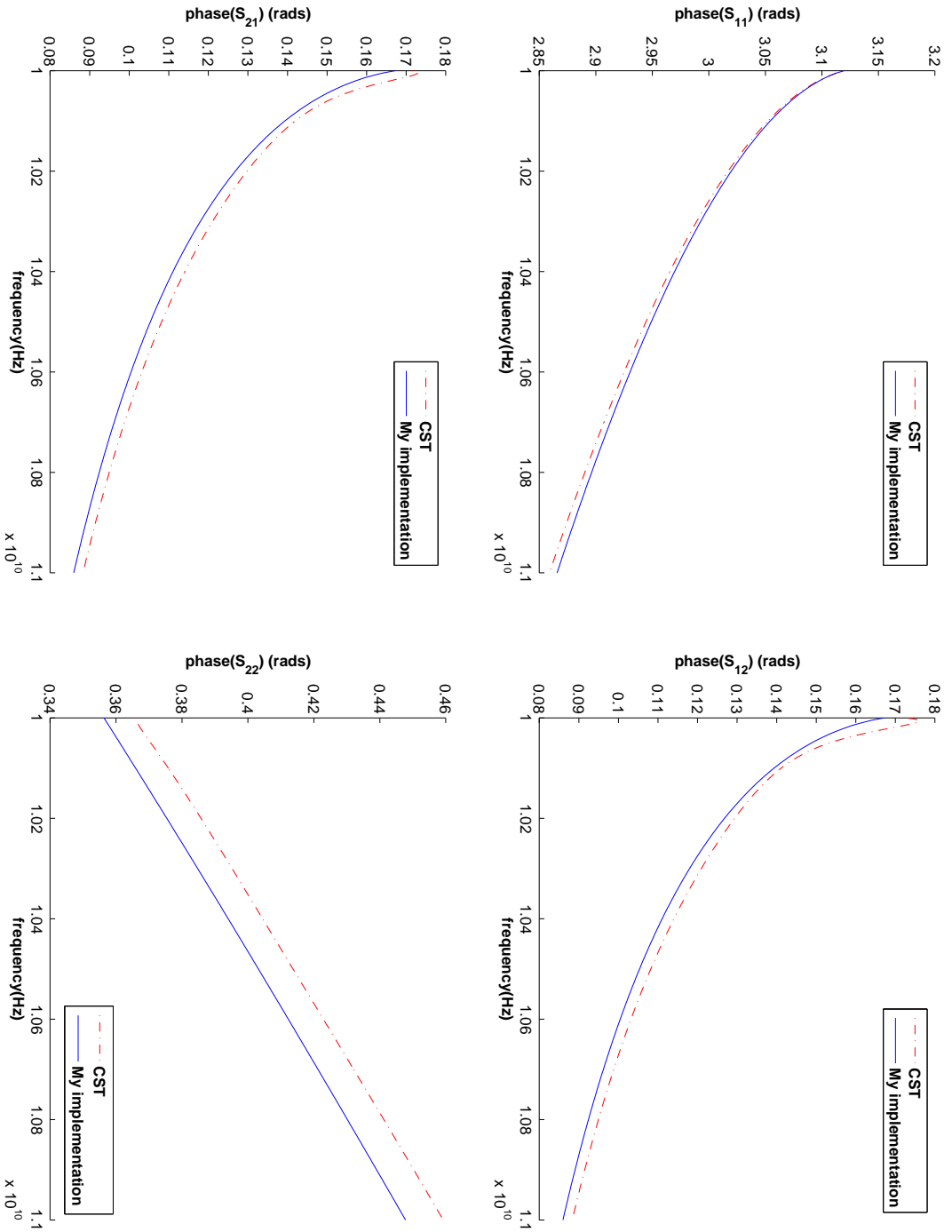


Figure 3.6: Phase of the S-parameters for a single step.

3.6. STUDY CASE: H-PLANE RECTANGULAR WAVEGUIDE PROBLEMS27

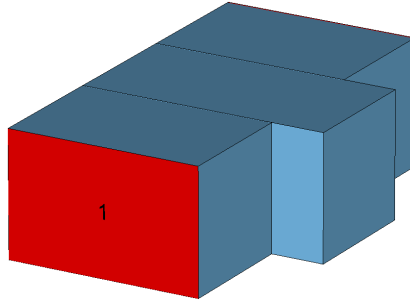


Figure 3.7: Two steps. Misaligned guides.

	Thickness (mm)		Longitude (mm)
Iris 1	8.60	Resonator 1	11.70
Iris 2	7.70	Resonator 2	13.10
Iris 3	7.30	Resonator 3	13.70
Iris 4	7.20	Resonator 4	13.80
Iris 5	7.20	Resonator 5	13.70
Iris 6	7.30	Resonator 6	13.10
Iris 7	7.70	Resonator 7	11.70
Iris 8	8.60		

Table 3.1: Band-pass filter measurements [7].

- Cut-off frequencies: $f_{c1} = 16.3GHz$, $f_{c2} = 17.7GHz$.
- Order: $N = 7$.
- Response type: Chebyshev
- Iris width: $2mm$.

The waveguide structure is depicted in Figure 3.10 on page 30 and the dimensions of each element can be found in Table 3.1.

After computing the filter response with the Mode-Matching software the results obtained are very close to the ones presented in [7] (obtained with the commercial tool CST Microwave Studio) as it can be checked at Figure 3.11 on page 31.

This test involved the characterization of the steps and also the cascading of their respective GSM. Thus it is a complete test that provides reliability to the developed code.

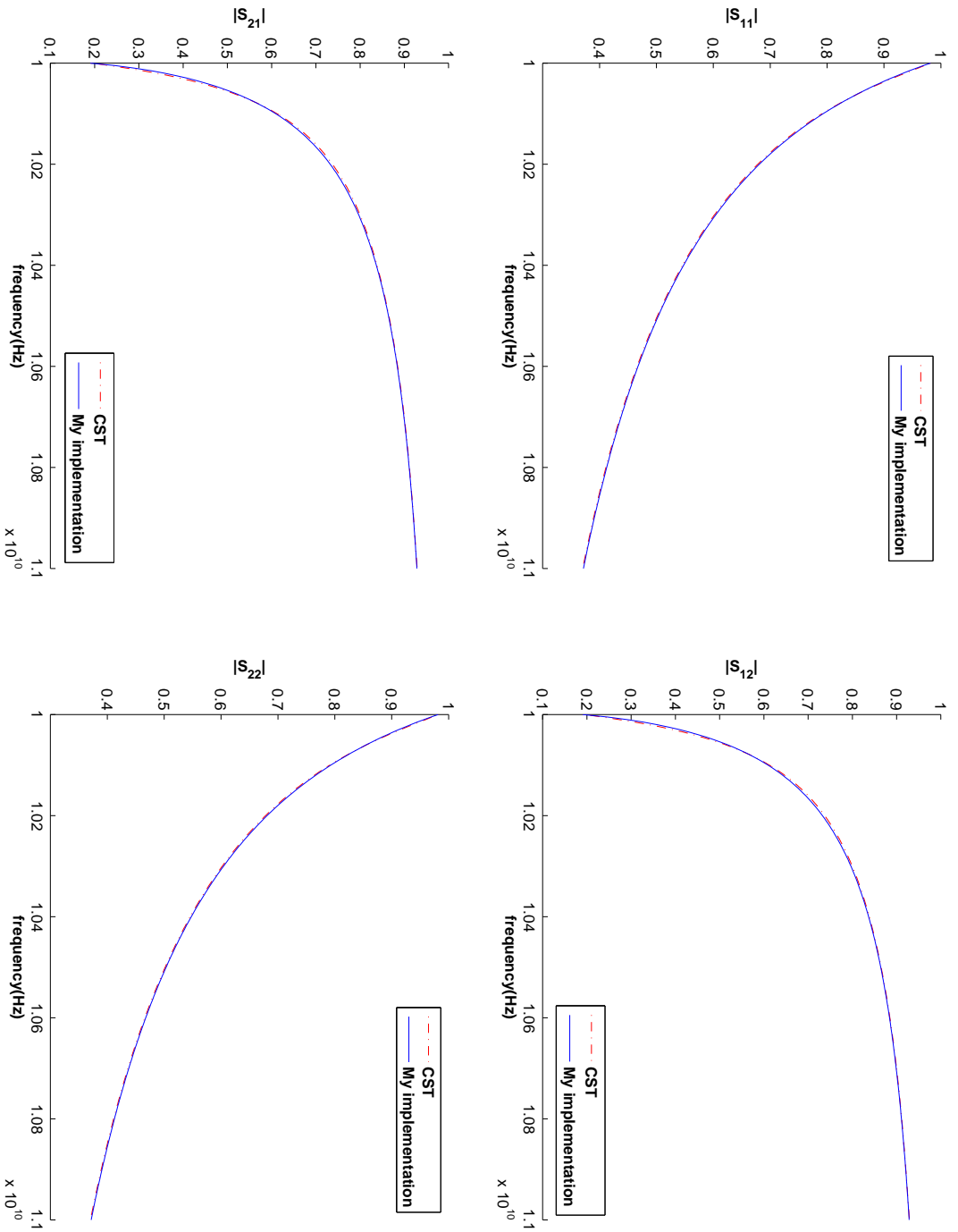


Figure 3.8: Module of the S-parameters for two steps.

3.6. STUDY CASE: H-PLANE RECTANGULAR WAVEGUIDE PROBLEMS29

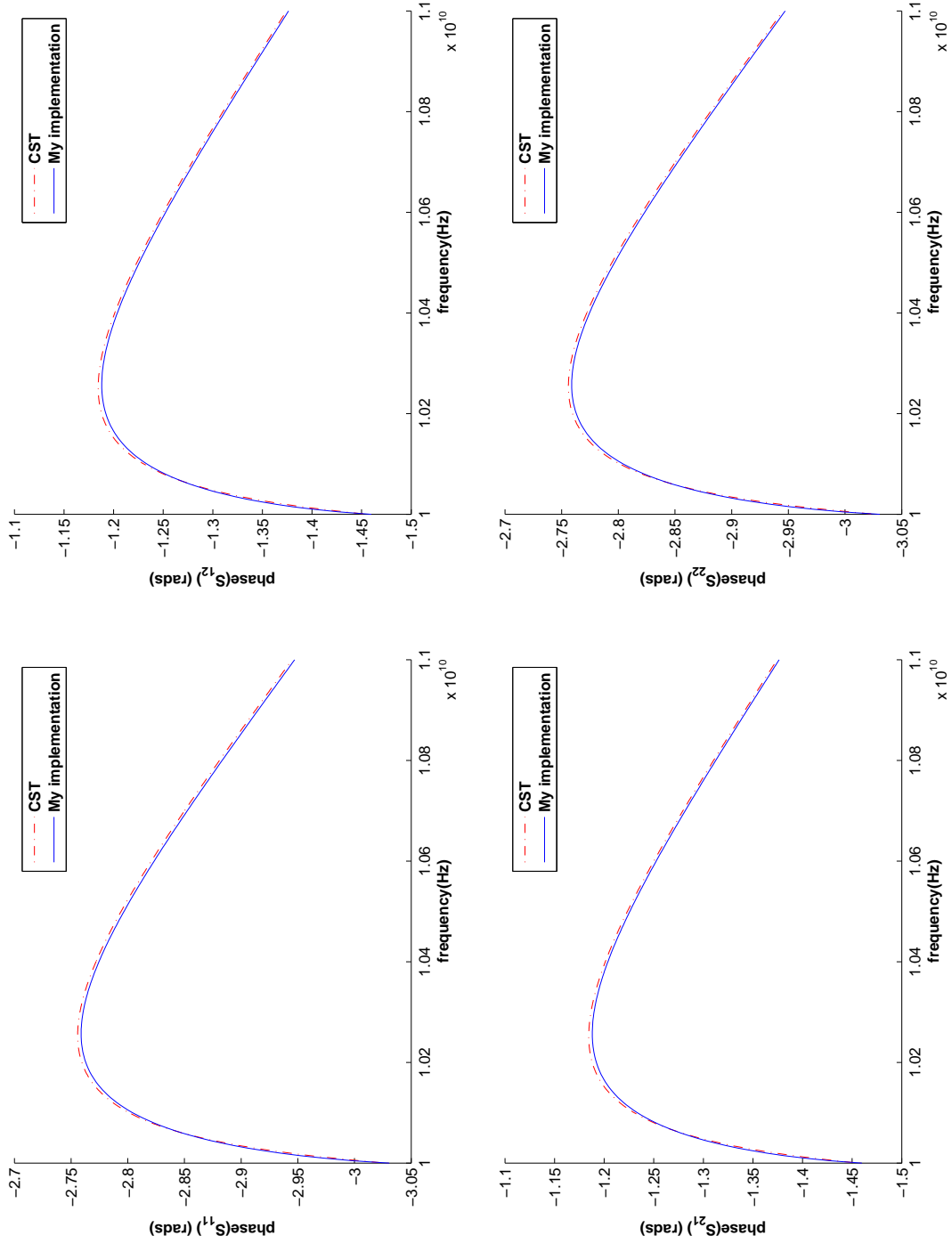


Figure 3.9: Phase of the S-parameters for two steps.

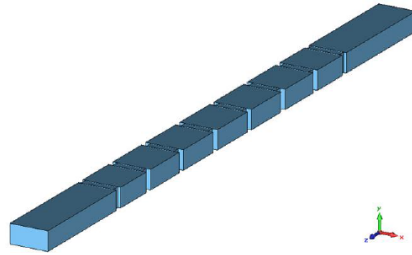


Figure 3.10: Band-pass filter representation [7].

3.7 Conclusions

The key idea of the Mode-Matching method is to characterize each one of the waveguide discontinuities making up a device by a matrix. Then a global characterization matrix of the whole device can be computed by cascading the partial matrices. This method takes into account not only the propagating modes at the waveguide device but also the high order evanescent modes that appear at the discontinuities. This evanescent modes are not taken into account by traditional equivalent circuit models.

As an illustration of the usefulness of a Mode-Matching implementation we have shown the simulation results for a single waveguide step, the concatenation of two steps and a real band-pass filter compound by resonant waveguide cavities. All these examples have been computed by a MATLAB code completely developed in this work.

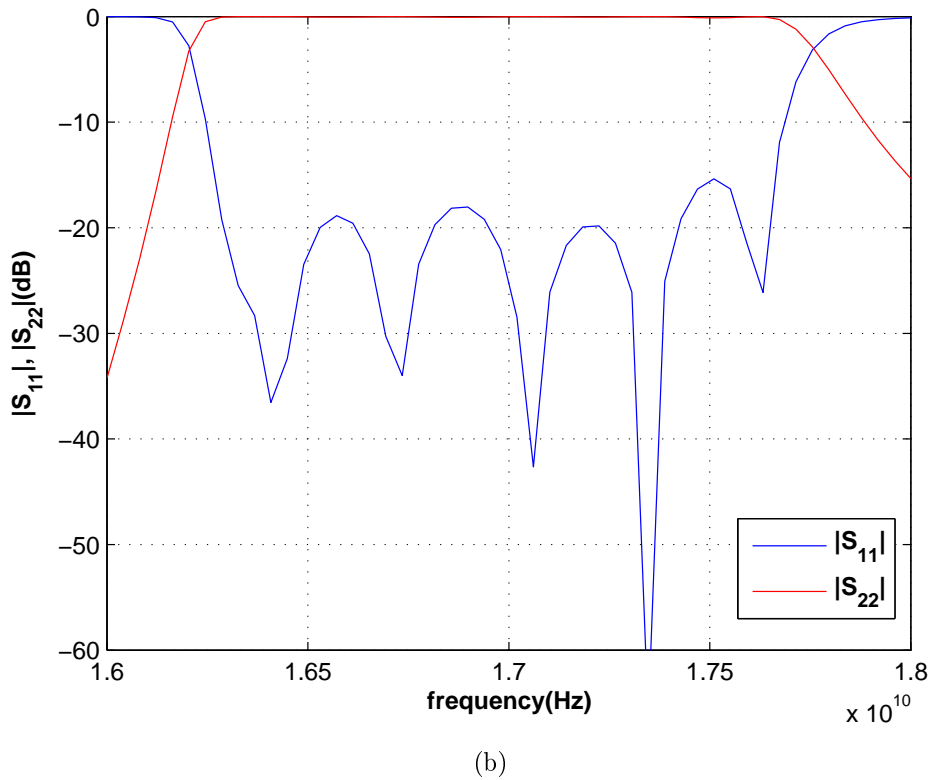
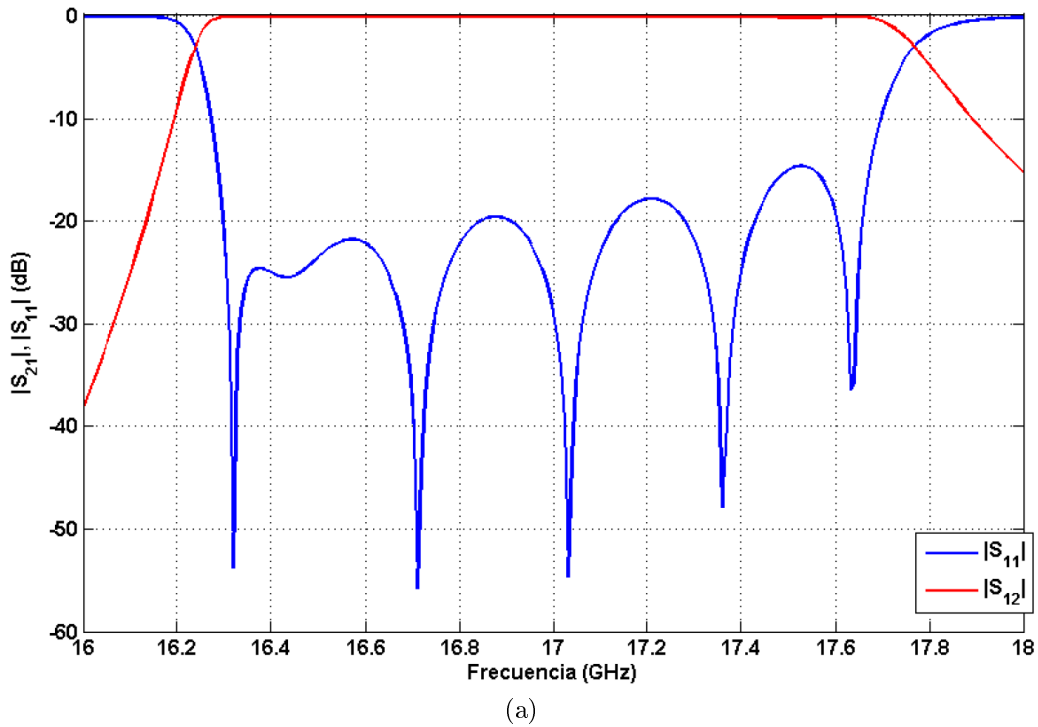


Figure 3.11: Comparison between the results obtained by [7] (3.11a) and the results obtained by the mode-matching software (3.11b)

Chapter 4

Modeling Horns

4.1 Motivation

Horn antennas have some properties that make them specially useful for both the ground and flight segment of satellite systems. They present higher gains, wider bandwidths and less losses (almost negligible if the dielectric filling the horn is air) compared with other types of antennas. Because of their construction they are also very robust and can be mounted on the fuselage of an airplane or on-board satellite.

The main problem with horns is that, since they are 3D¹ antennas, simulation times are usually large when using a general numeric method. Unfortunately most of the commercial software tools implement general numeric methods.

The objective of this work is to improve the simulation times by using the mode-matching method to model a horn as a succession of discontinuities.

4.2 Stage 1: Inside the horn

As stated before, the key idea of the method is to model the horn as a succession of waveguide steps and then use a Mode-Matching software to simulate it. This process will provide the amplitudes of the modes at the aperture of the horn, which will be used in the next section to compute the radiation pattern. Since developing an efficient and quick mode-matching

¹All antennas are in reality 3D objects, but wire antennas like dipoles are considered to be 1D and planar antennas like patches to be 2D.

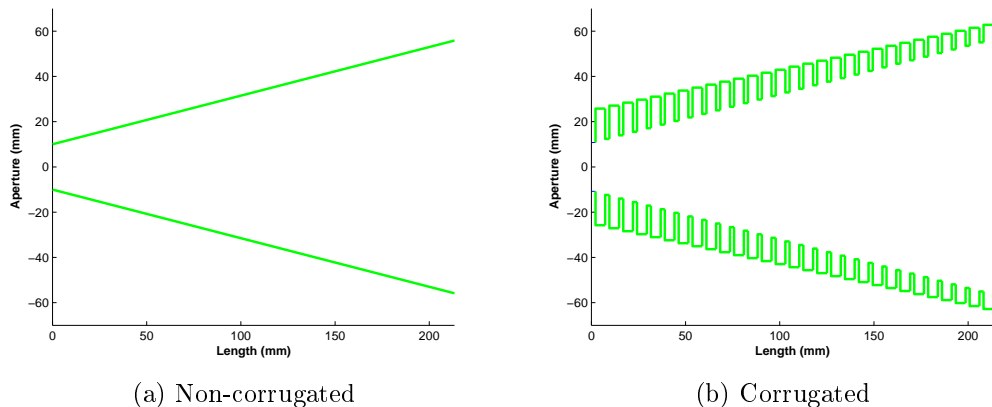


Figure 4.1: Profile of different horn types.

software for hundreds of waveguide steps with circular waveguides would be beyond the scope of this work, an implementation created by the RFCAS research group will be used.

In any case, at the previous chapter the results of a software fully developed in this work were presented. This code analyzes a subset of the waveguide discontinuity problems and implements the same mode-matching technique. However, the code provided by RFCAS is a compiled executable file that has been optimized for speed when dealing with hundreds of discontinuities. This optimized code was out of the scope of this work, and, since the fundamentals of the method were already covered in previous chapter, we believed that it was a better strategy to focus in the final problem (the horn), rather than developing again an optimized code.

The next problem that must be faced is the horn modeling. This task depends on the type of horn under study. This work only considers circular horns. In addition to the shape, horns can be classified as corrugated or non-corrugated (see Figure 4.1). With corrugated horns the modeling is easy since by their own nature they are already “discrete”. Each of the corrugations can be considered as a waveguide step.

The troubles appear when dealing with a non-corrugated horn. Two different methods have been implemented as a MATLAB script to accomplish the task of computing the discrete version of this type of antenna. They will be called the “hold” and the “middle-point” methods and a depiction of both can be found at Figure 4.2 on page 36. Both methods divide the

profile in sections of constant length. These sections will correspond with the waveguide sections of the discrete model. The radius associated with each section is computed differently by each discretization method. The “hold” method assumes that the waveguide section radius is equal to the radius of the horn at the section end that is closest to the waveguide input. The “middle-point” method obtains the horn radius at both ends of the interval and then computes the waveguide section radius as the average of these two values.

The “hold” method may introduce greater error since it is representing some regions of the physical structure smaller than they really are and other regions are represented bigger, this is specially important when dealing with narrow band problems like some types of filters where such kind of error can significantly displace the frequency response. In this kind of problems the “middle-point” method performs better, but since horn antennas are usually wide band devices the two methods give similar results at the problems under study, as it will be shown later.

It is important to note that convergence of the results must be studied by increasing the number of steps in which the horn is divided until it is noticed that the differences at the results become insignificant for the application under study. This convergence study must be also carried out for the number of modes used at the Mode-Matching simulation. Examples of these two types of convergence will be seen in next chapter.

4.3 Stage 2: Outside the horn

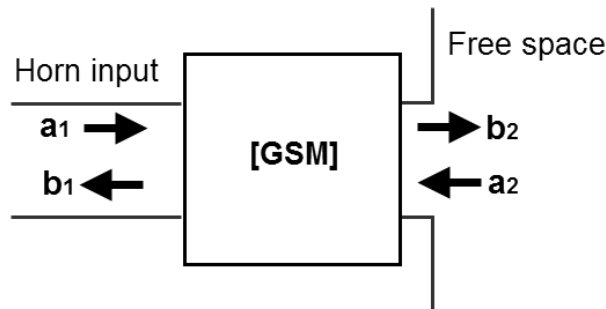
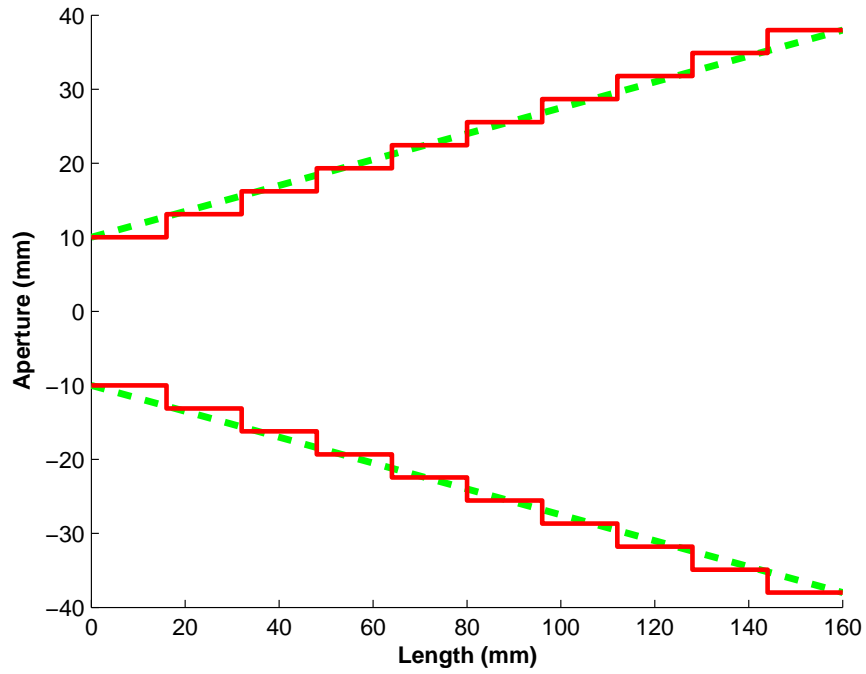
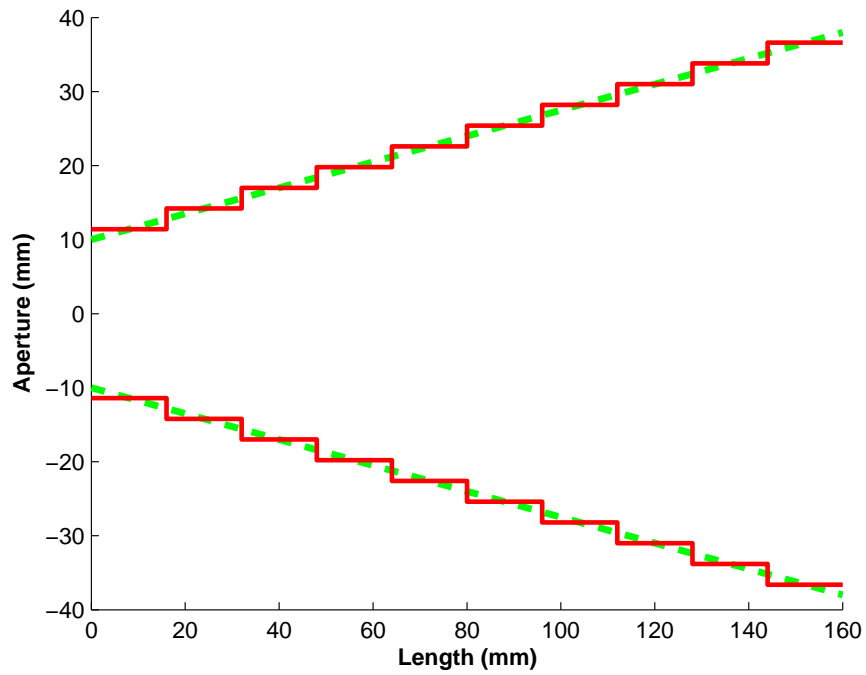


Figure 4.3: Horn antenna characterized by its GSM.



(a) Hold method



(b) Middle-point method

Figure 4.2: Representation of the two methods used to model a smooth horn. Dashed green shows the real profile and solid red the discrete one.

The previous step provides with an array of coefficients representing the amplitudes of the modes at the horn aperture. These modes can be used to compute the radiation pattern for the antenna under study. First of all, the total electric field at the horn aperture has to be obtained. It can be obtained as:

$$\vec{\mathbf{E}}_{ap} = \begin{cases} \sum_m \{ A_m^{TE} \vec{\mathbf{e}}_m^{TE} + A_m^{TM} \vec{\mathbf{e}}_m^{TM} \} & 0 \leq r \leq a \\ 0 & \text{otherwise} \end{cases}, \quad (4.1)$$

where a is the aperture radius and A_m^{TE}, A_m^{TM} and $\vec{\mathbf{e}}_m^{TE}, \vec{\mathbf{e}}_m^{TM}$ are the amplitudes (referred as b_2 at Figure 4.3) and the modes scattered at a discontinuity as expressed in (3.2) and (3.3) respectively. The TE modes have been separated from the TM to simplify notation in the following integrations². To obtain the radiated field at the far-field region the transverse field must be integrated at the aperture [6, 5]:

$$\vec{\mathbf{E}} = \frac{jk e^{-jkr}}{4\pi r} (1 + \cos(\theta)) a \int_0^1 \int_0^{2\pi} \vec{\mathbf{E}}_{ap} e^{jkarsin(\theta)\cos(\phi-\phi')} r dr d\varphi \quad (4.2)$$

The calculation of this integral is not presented here since it is very complex. The interested reader may find it in [5]:

$$E_\theta = \frac{k e^{-jkr}}{2r} (1 + \cos(\theta)) a^2 \sin(\phi) \sum_m [A_m^{TE} K_m^{TE} j J_1(p'_{1m}) \frac{J_1(kasin(\theta))}{kasin(\theta)} - A_m^{TM} K_m^{TM} j p_{1m} J'_1(p_{1m}) \frac{ka J_1(kasin(\theta))}{(p_{1m})^2 - (kasin(\theta))^2}] \quad (4.3)$$

$$E_\phi = \frac{k e^{-jkr}}{2r} (1 + \cos(\theta)) a^2 \cos(\phi) \sum_m [A_m^{TE} K_m^{TE} (p'_{1m})^2 J_1(p'_{1m}) \frac{J'_1(kasin(\theta))}{(p'_{1m})^2 - (kasin(\theta))^2}] \quad (4.4)$$

The radiation intensity can be computed as:

²For the problem under study only the TE_{c1r} and TM_{s1r} modes are used. These are the only modes that have to be considered if the horn is excited only with the fundamental mode at the input waveguide. Its field expression can be found in [3]

$$U = \frac{r^2}{2\eta} [|E_\theta|^2 + |E_\phi|^2] \quad (4.5)$$

And the directivity as:

$$D = \frac{4\pi U_{Max}}{P_{rad}} \quad (4.6)$$

Where P_{rad} can be obtained from the GSM as³:

$$P_{rad} = 1 - |S_{11}^{GSM}|^2. \quad (4.7)$$

This last equation assumes that the horn is lossless.

4.4 Conclusions

At this section we have shown how to obtain the radiation pattern of a horn antenna by means of the Mode-Matching method. It is necessary to obtain first a discrete model of the antenna representing a succession of waveguide steps. Using a Mode-Matching software the modal amplitudes at the horn aperture can be obtained. These modal amplitudes can be used to compute the radiation integrals that finally give the radiated far field.

For accomplishing this we have implemented two different discretization methods that provide with a model of the antenna under study and we also coded a MATLAB program that computes the radiation integrals and directivity values. The only code used and not developed by us was the one that carries out the Mode-Matching analysis. Since developing a full functional and optimized Mode-Matching software would be out of the scope of this project we used an implementation created at the RFCAS research group. In any case, as it was shown in the previous chapter, we developed a Mode-Matching code for analyzing a subset of the waveguide step problems using the same type of technique.

³If the modes have been normalized as stated by 3.23 on page 23 and $Q = I$ then P_{rad} should also be divided by 2. Note that in the Poynting theorem there is a factor of two dividing the surface integral.

Chapter 5

Verification cases

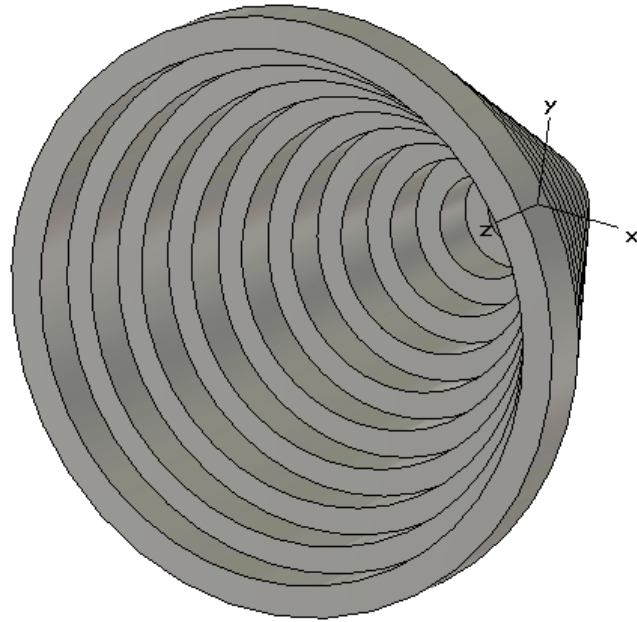
5.1 Motivation

This chapter is devoted to verify the analysis method that has been implemented. In order to make this check, some horns whose radiation pattern was known in advance have been simulated. The results obtained by the developed code are compared with those obtained from other numerical methods, including commercial software, and measured results coming from actual devices on-board satellites, by other authors.

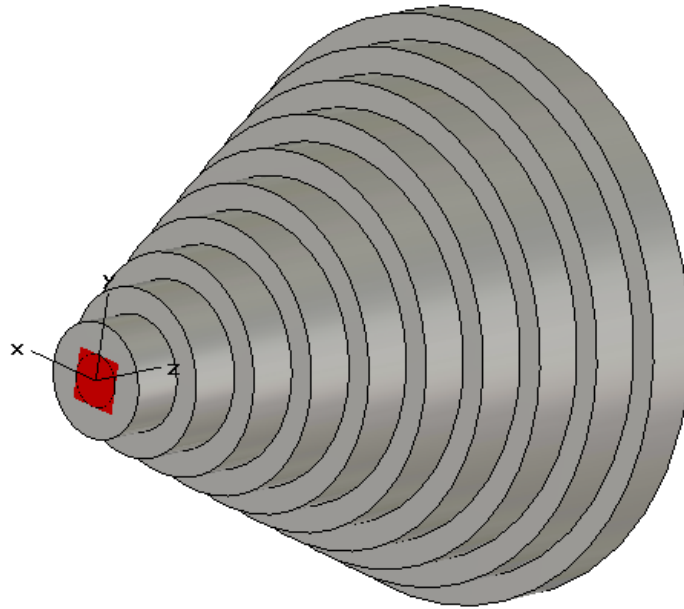
5.2 Tercius

Tercius could barely be called a horn antenna. It is more like some waveguide steps put together but, fortunately, it radiates and was simple enough to be simulated with CST Studio in order to get a first reference antenna to test the code. The dimensions of each waveguide section can be found at Table 5.1 on page 41.

Simulating this antenna with CST took two hours, while simulation with the mode-matching software took less than a minute using the same computer. In the spite this is not a real performance test, the comparison should at least give some insight of the advantages obtained by using mode-matching rather than general numerical methods, when the structure under analysis is



(a)



(b)

Figure 5.1: 3D representation of Tercius

Radius (mm)	Length(mm)
5	10
10	10
15	10
20	10
25	10
30	10
35	10
40	10
45	10
50	10

Table 5.1: Dimensions of the waveguide steps (10 waveguide sections) at Tercius.

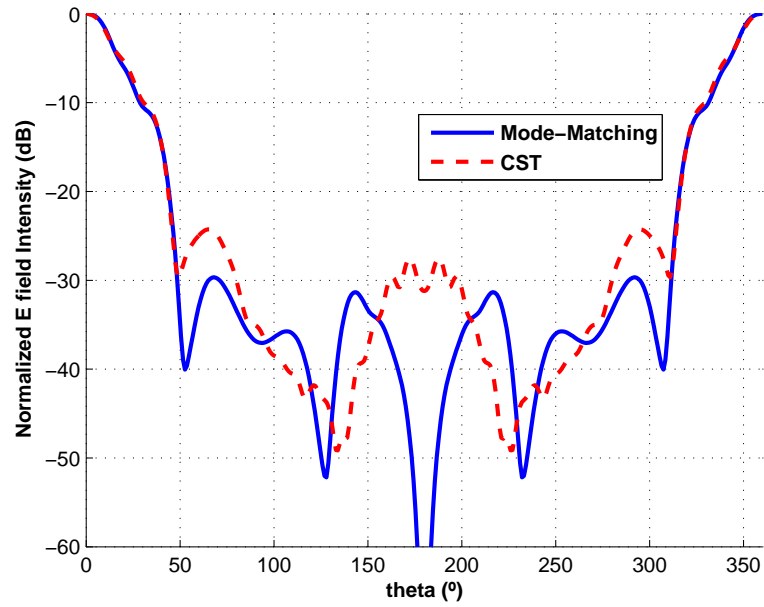
suitable for a mode-matching analysis. The number of modes considered at the input waveguide and at the aperture were 7 and 70 respectively.

The results of the radiation pattern are depicted in Figure 5.2 on the next page superimposed onto the radiation pattern obtained with CST. It can be seen that the results for the main lobe are almost identical and they start to diverge at the first side lobe. It should also be considered that the formulas used only work for $-90^\circ \leq \theta \leq 90^\circ$. Since horn antennas are very directive these should not be an issue for more practical cases. The reason for this difference is that the used formula (4.2) for the radiated field is less accurate in the regions close to the horn aperture [6, 5, 2].

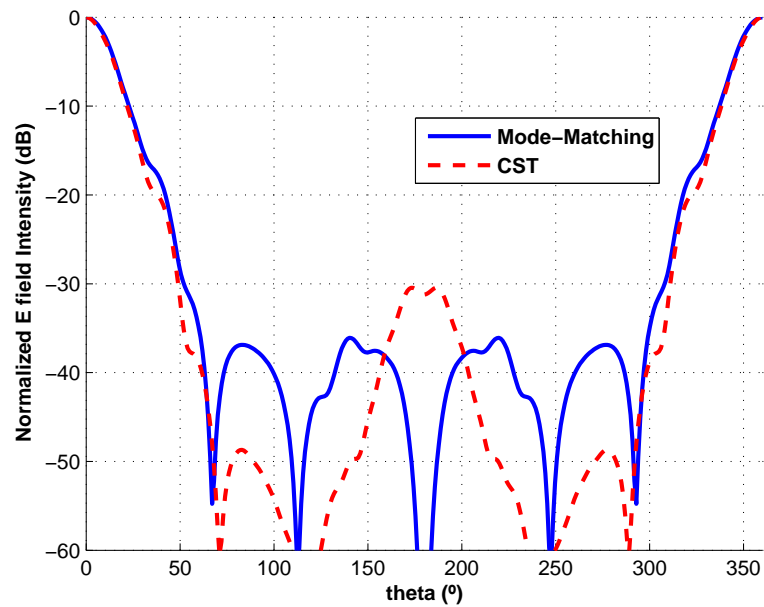
5.3 Hispasat 1C

After a first verification using a simple antenna simulated with CST Studio it is time to try working with a real world antenna. The selected horn is the actual antenna used at the Hispasat 1C satellite. Since obtaining a reference model by means of a simulation via CST Microwave Studio would be practically impossible with the computers available to us, the Mode-Matching results will be compared with those obtained by [8] using graphical superposition.

The profile of the antenna can be seen at Figure 5.3 on page 44, hav-



(a) E-Plane($\phi = 90^\circ$). $D_{0,MM} = 16.58dB$.



(b) H-Plane($\phi = 0^\circ$). $D_{0,MM} = 16.58dB$.

Figure 5.2: Tercius radiation pattern. Comparison between Mode-Matching computation and CST Studio Microwave.

ing a look at it may reveal why this particular horn was chosen: it has the type of profile suitable for mode-matching analysis. When using a numerical method implemented on a computer to analyze a real world object, convergence problems can appear at the results from two main sources. It may be that the numerical method it is not properly implemented or it may be that the discrete representation of the real world (therefore continuous) object that is being used has not enough resolution.

As stated before corrugated horns can be easily modeled as the cascading of the waveguide steps created by the corrugations. So the antenna under study is complex enough to challenge the Mode-Matching technique but permits avoiding the problem of sampling the profile, avoiding therefore one of the error sources. Therefore this horn is modeled as 222 waveguide sections. The number of modes considered at the input waveguide and at the aperture were 14 and 70, respectively. The ratio between these two numbers is the ratio between the radius of the aperture and the radius of the input waveguide. In the other circular waveguide sections of the horn, the number of modes is the result of multiplying the number of modes in the aperture times the radius of the circular waveguide under analysis over the radius of the aperture [4].

Radiation patterns for the two studied frequencies can be seen in Figure 5.4 on page 45 and Figure 5.5 on page 46, where the Mode-Matching data corresponds to the dashed red curve. Directivity obtained by [8] can be seen at the data box on the graph while the values computed by Mode-Matching can be seen at the picture caption for each plane.

The return losses have also been computed using the Mode-Matching software. The reference values for checking this computation have been extracted from [6]. This comparison is shown at Figure 5.6 on page 47. It can be seen that the radiation pattern results converge using in the simulation 70 modes at the horn aperture. However the return loss computation requires considering more modes to reach convergence.

It is clear that the results obtained by simulating the horn using the Mode-Matching implementation agree with those presented by the original author. The computation times were around one and two minutes, while simulating this horn with CST Microwave Studio using the same computational resources would have taken a large amount of time.

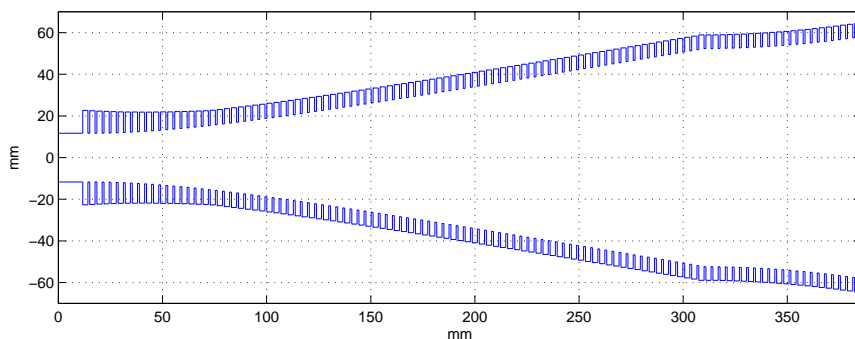


Figure 5.3: Profile of the Hispasat 1C

5.4 Conical Horn

Having tested that the Mode-Matching implementation is working precisely now it is time to attempt simulating a smooth antenna. In this case, another additional issue has to be faced: the discretization of the horn profile. In order to start with an easy example a simple conical horn has been chosen, which means that its profile (as can be seen at Figure 5.7a on page 48) has a single slope. The sampling method implemented uses just a continuous spacing along the horn length. Of course, the discrete representation depicted at the figure has a low number of steps (ten) so the idea of the sampling process can be seen. A real model requires higher resolution. In this case, 100 waveguide sections were used. The number of modes considered at the input waveguide and at the aperture were 18 and 70, respectively.

The horn design as well as the reference radiation patterns have been obtained from [9] but since this reference does not provide a value for the antenna directivity, this parameter has been checked against the results provided by [6]. At Figure 5.8 on page 49 it is shown the obtained radiation pattern (solid thick blue) compared with the reference values. The directivity values obtained with Mode-Matching are the same as those referred in [6].

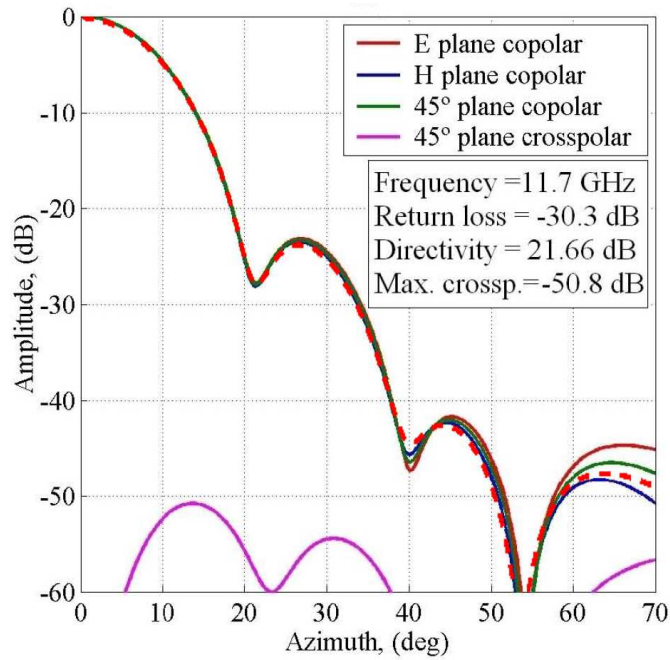
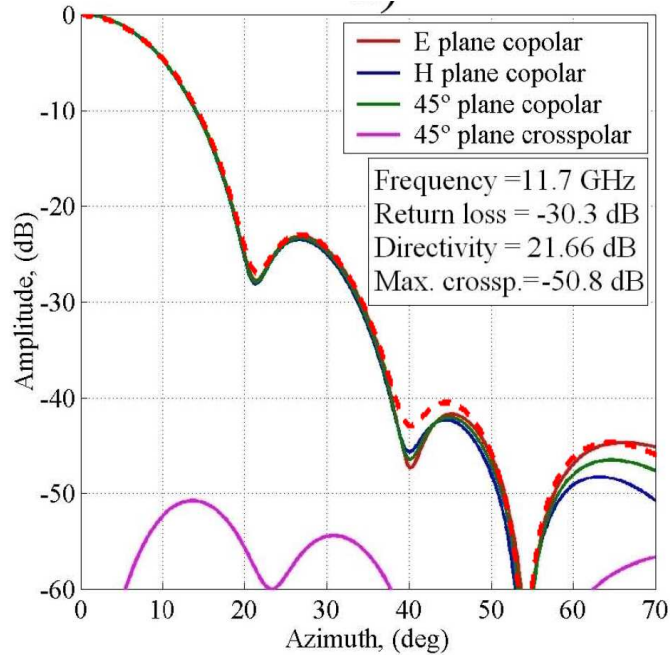
(a) E Plane($\phi = 90^\circ$). $D_{0,MM} = 21.67dB$.(b) H Plane($\phi = 0^\circ$). $D_{0,MM} = 21.67dB$.

Figure 5.4: Hispasat 1C horn radiation pattern. $f = 11.7GHz$. Mode-Matching results (dashed red) of this work are superimposed on the graphs provided by [8].

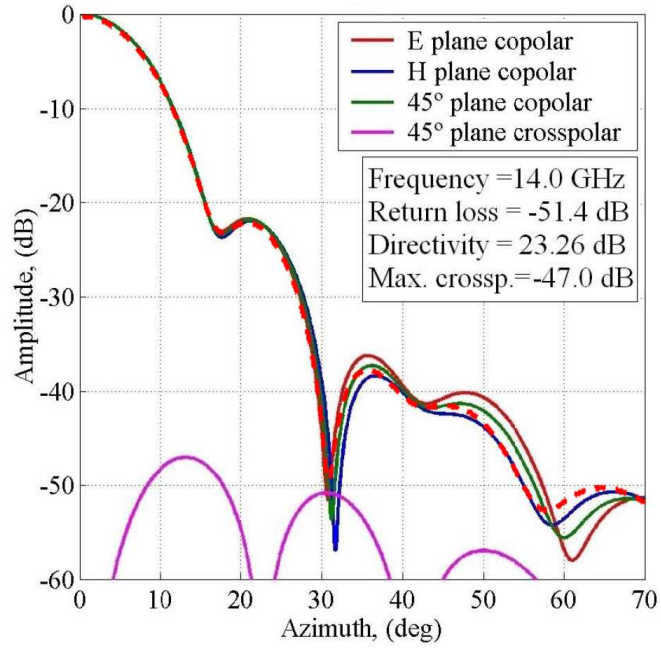
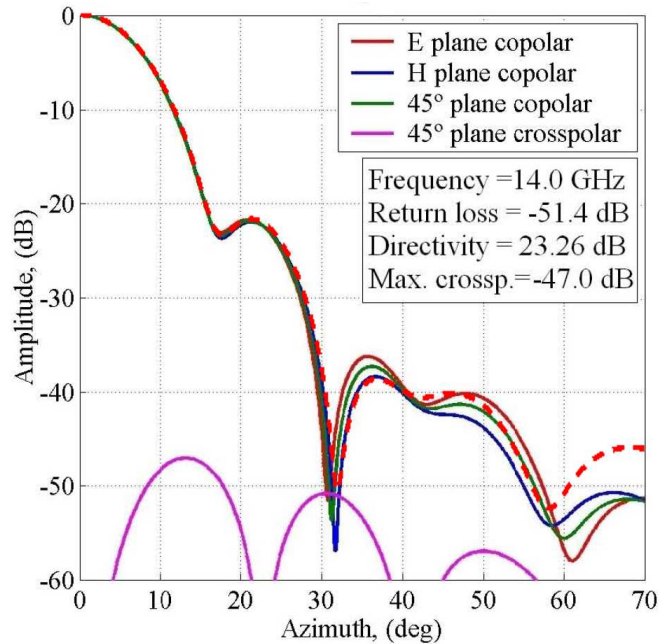
(a) E Plane($\phi = 90^\circ$). $D_{0,MM} = 23.26dB$.(b) H Plane($\phi = 0^\circ$). $D_{0,MM} = 23.26dB$.

Figure 5.5: Hispasat 1C horn radiation pattern. $f = 14GHz$. Mode-Matching results (dashed red) of this work are superimposed on the graphs provided by [8].

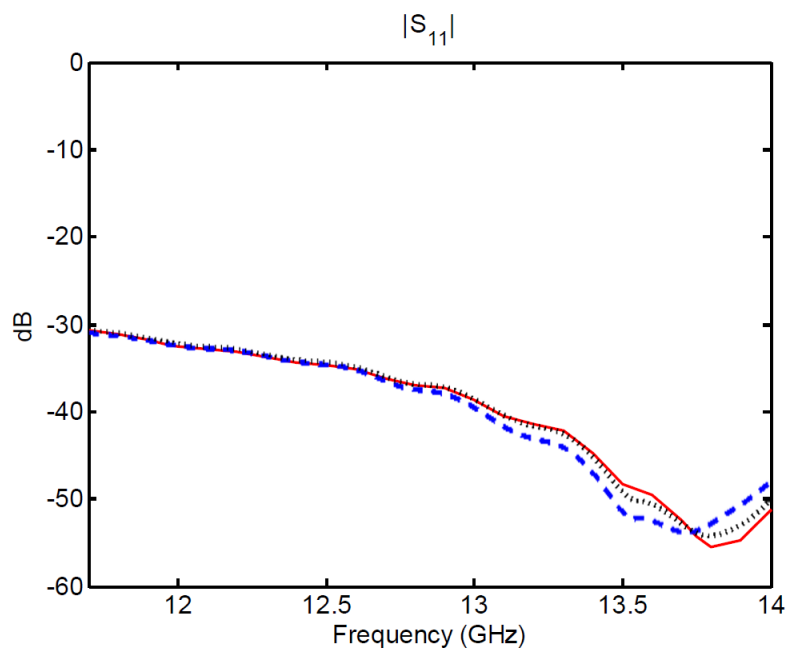
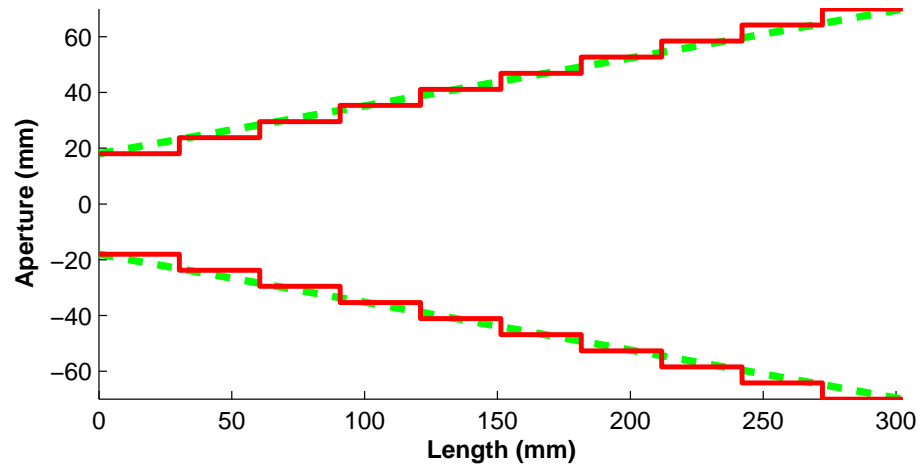
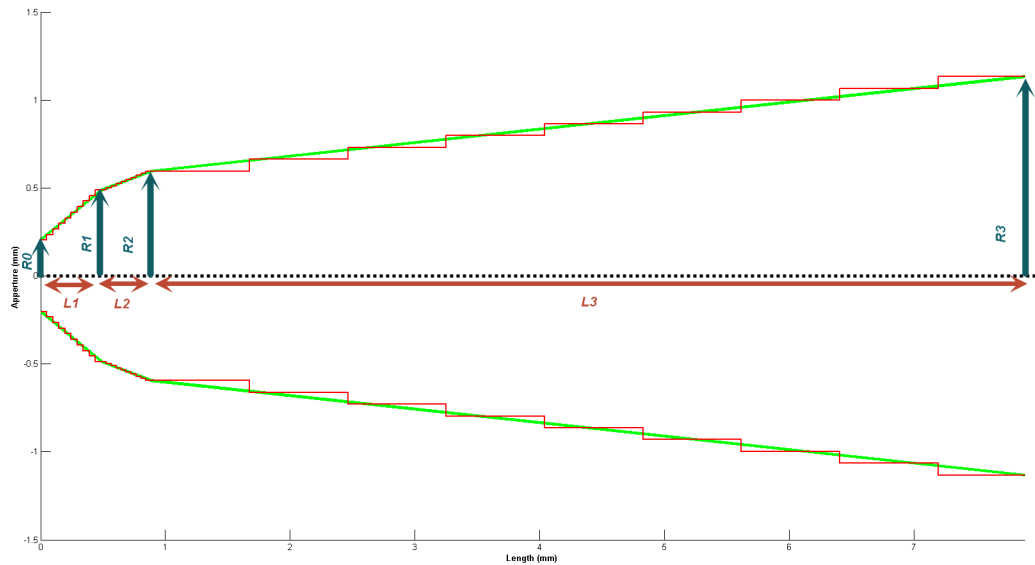


Figure 5.6: Return loses of the Hispasat 1C. Solid red: Reference [6]. Dashed blue: Mode-Matching with 70 modes at the aperture. Dotted black: Mode-Matching with 120 modes at the aperture.

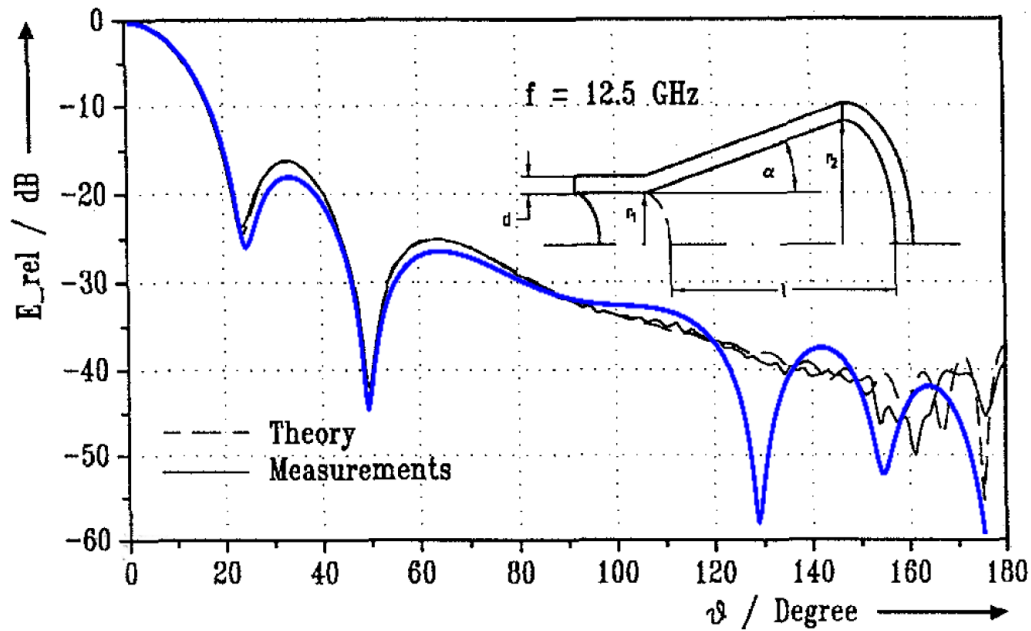
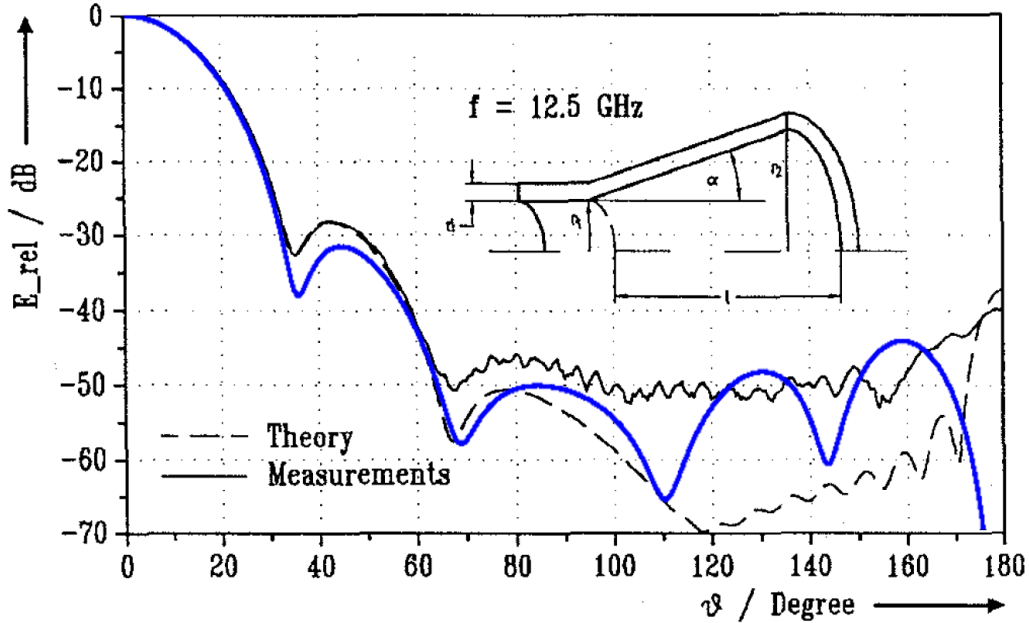


(a) Profile of the conical horn. Waveguide radius: 18mm . Horn aperture: 70mm . Length: 302.5mm .



(b) Profile of the High Performance Feed Horn. Dimensions R_0 , R_1 , R_2 , R_3 , L_1 , L_2 and L_3 have been extracted from [10]. Red stairs represent the discrete version of the horn. Low resolution has been used so the steps are easily visible.

Figure 5.7: Discretized profile of different horns

(a) E Plane($\phi = 90^\circ$). $D_{0,MM} = 18.50dB$.(b) H Plane($\phi = 0^\circ$). $D_{0,MM} = 18.50dB$.Figure 5.8: Conical Horn simulation (blue, thick) compared with theoretical and measured data from [9] (black, thin). $f = 12.5GHz$.

	Radius (mm)		Lengths (mm)
R0	0.203	L1	0.487
R1	0.488	L2	0.398
R2	0.595	L3	7.886
R3	1.2		

Table 5.2: Measurements of the High Performance Feed Horn [10].

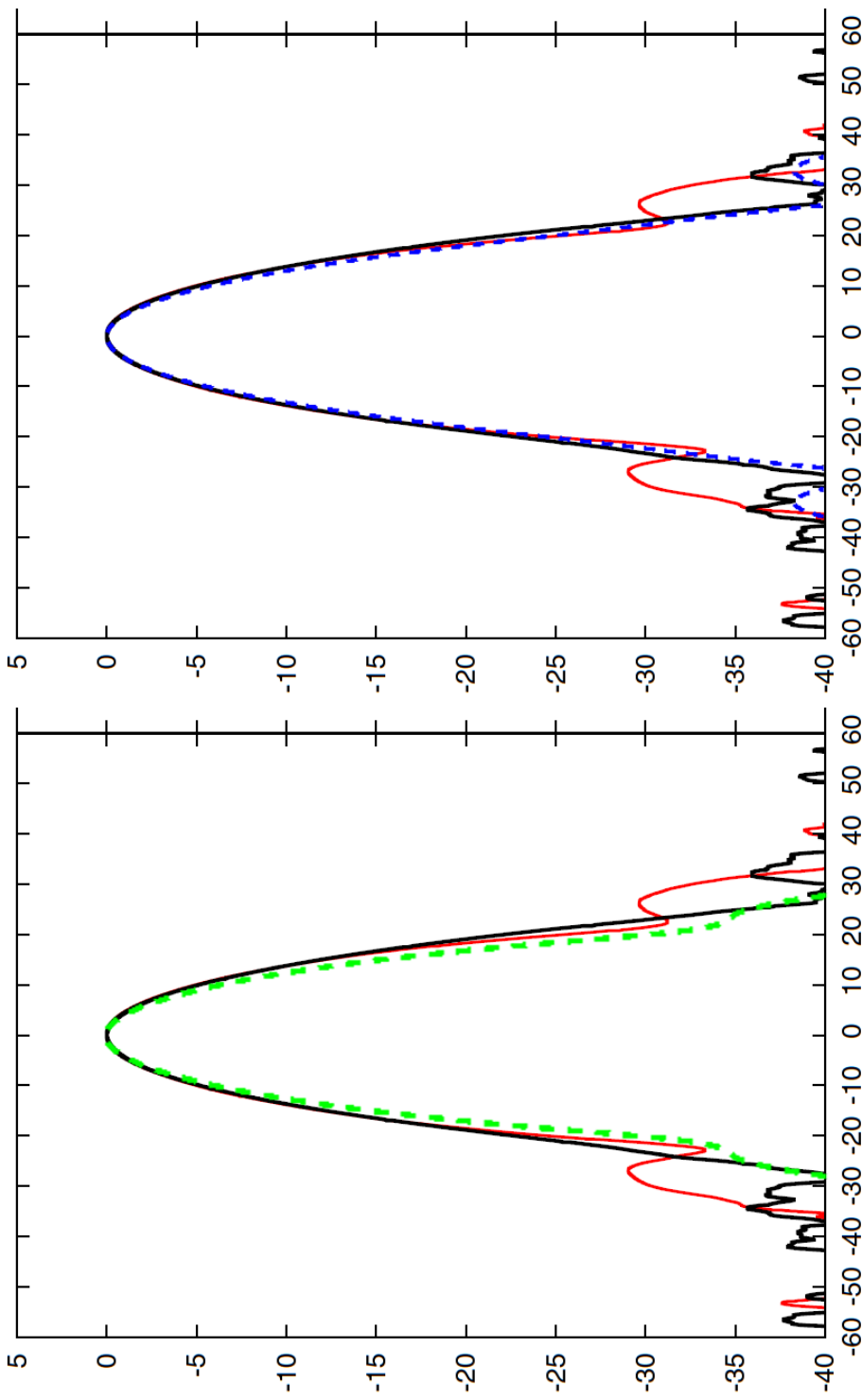
5.5 High Performance Feed Horn

The last verification case is a smooth horn with three sections of different slope. This means that the horn profile can be divided in three regions of smooth continuous shape. In each region, the smooth profile is discretized as in the previous verification case. The reference design and measurements can be found at [10]. The profile of the antenna has been discretized using the same number of samples at each step as can be seen at Figure on page 48, where the dimensions can be found at Table 5.2. In this case 100 waveguide sections were used at each section, having then a total of 300 waveguide sections for the whole antenna. The number of modes considered at the input waveguide and at the aperture were 11 and 70, respectively. The obtained radiation pattern can be found at Figure 5.9 on the facing page superimposed onto the measurements by [10].

In general the obtained results match accurately with the measurements provided by the original author. The radiation pattern at the E-Plane obtained by Mode-Matching does not match very well with the original data at the side lobe. We attribute this to the fact that the comparison is performed against measured, where higher side lobe levels may appear due to manufacturing tolerances.

5.6 Convergence

All the verification cases have been presented in previous figures showing the final results, postponing the convergence study associated to the used numerical method to this section. The different sources of problems that have to be taken into account for this numerical method are analyzed now. In the implemented software, convergence is related to three different parameters: discretization method for the profile of the horn, number of waveguide steps



(a) E-plane. (Solid red: Measures. Dashed green: Mode Match-(b) H-plane. (Solid red: Measures. Dashed green: Mode Matching).

Figure 5.9: High performance feed horn simulation compared with measurement data by [10].

used to model the horn, and number of modes considered when performing the Mode-Matching analysis. The non-corrugated conical horn previously studied at this chapter has been used for the convergence analysis, computing its radiation pattern as well as its return losses for different simulation conditions. The conclusions obtained for this analysis could be also extended to the other verification cases.

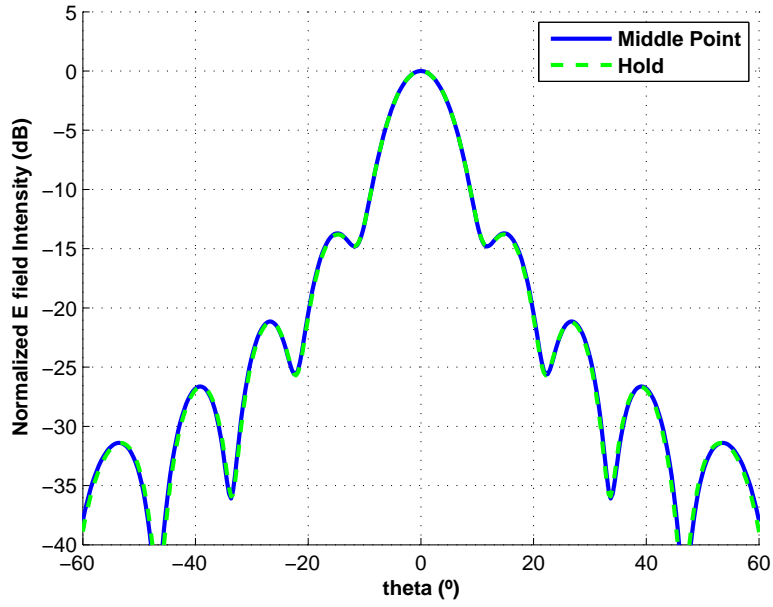
Looking at Figure 5.10 on the next page and Figure 5.13a on page 56 it can be seen that, as stated at chapter 3, the discretization method used to model the horn antenna does not suppose a significant difference on the results. The number of modes at the aperture and the number was 70 and the number of steps while discretizing were 100 (for the radiation pattern) and 160 (for the return losses).

Figure 5.11 on page 54 and Figure 5.13b on page 56 show a convergence study for different number of modes used at the Mode-Matching analysis. The number of modes presented at the figure legend makes reference to the number of modes at the horn aperture. The number of modes at each waveguide step is computed accordingly to the waveguide radius at the discontinuity. As it can be seen, increasing the number of modes gives a more accurate computation of the side lobes but does not change significantly the main lobe. The discretization method used at this test was the “middle-point” with 100 steps for the radiation pattern and 160 steps for the return losses.

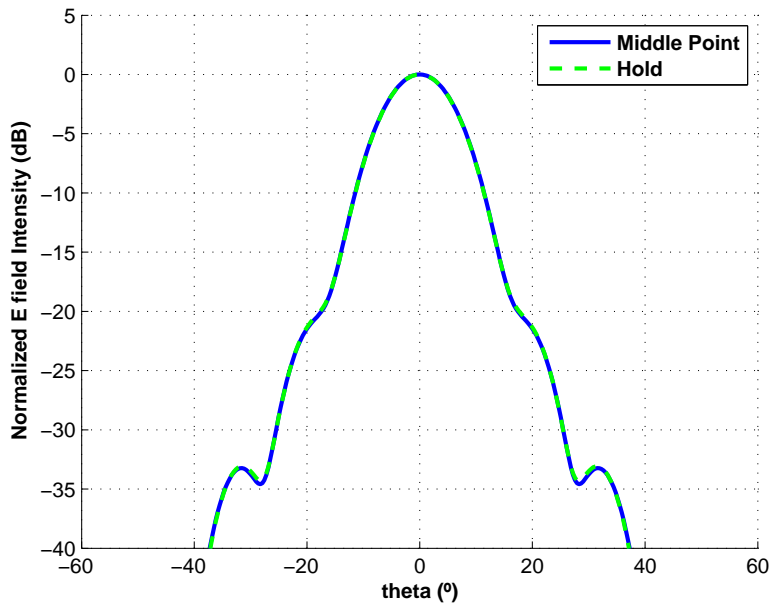
The last test studies how the number of waveguide steps used at the discrete model of the horn affect the convergence. Looking at Figure 5.12 on page 55 it can be seen that low values of this parameter give non satisfactory results not only at the side lobes but also at the main lobe. Convergence occurs for values around 100 steps. Figure 5.13c on page 56 shows that the number of waveguide sections also affects significantly to the accuracy of the return losses computation. The chosen discretization method was the “middle-point” and the number of modes at the aperture was 70.

5.7 Conclusions

Through this chapter it has been shown that the results obtained by the developed software match other simulations and measurements very accurately. This coincidence occurs specially at the main lobe, and the results start to diverge as θ grows. Since horn antennas are usually highly directive this should not be an issue for practical cases. Moreover, the advantage is clear:

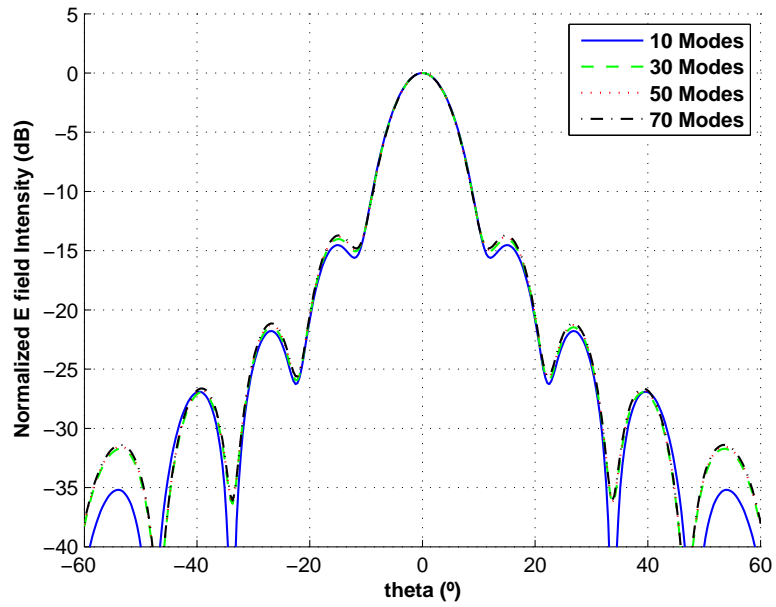


(a) E-Plane

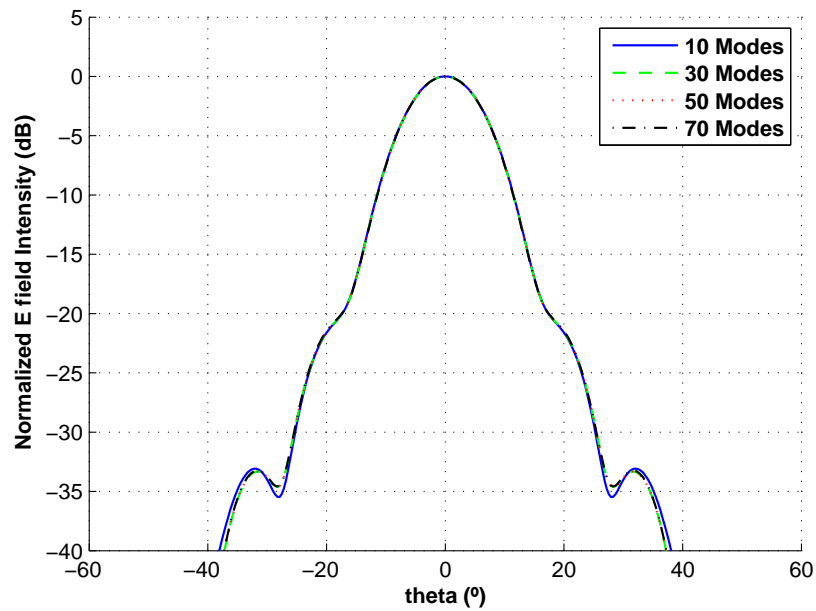


(b) H-Plane

Figure 5.10: Convergence of the radiation pattern for different discretization methods.

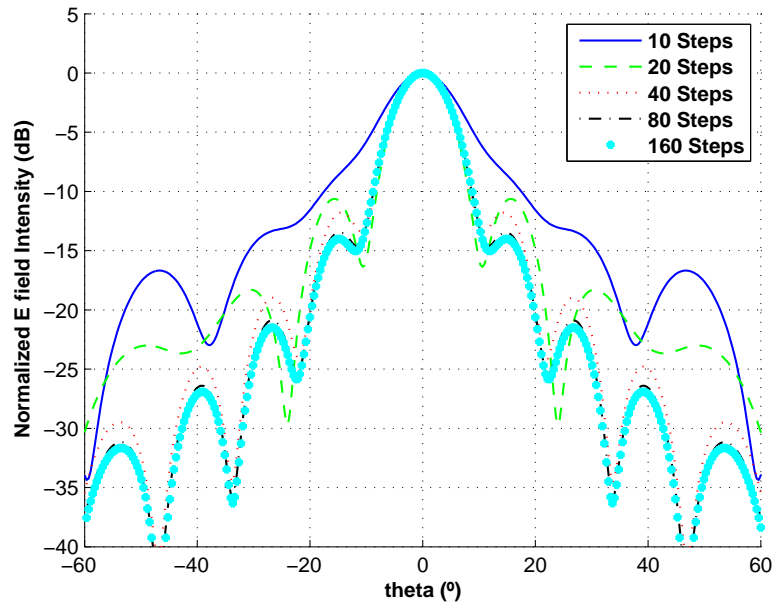


(a) E-Plane

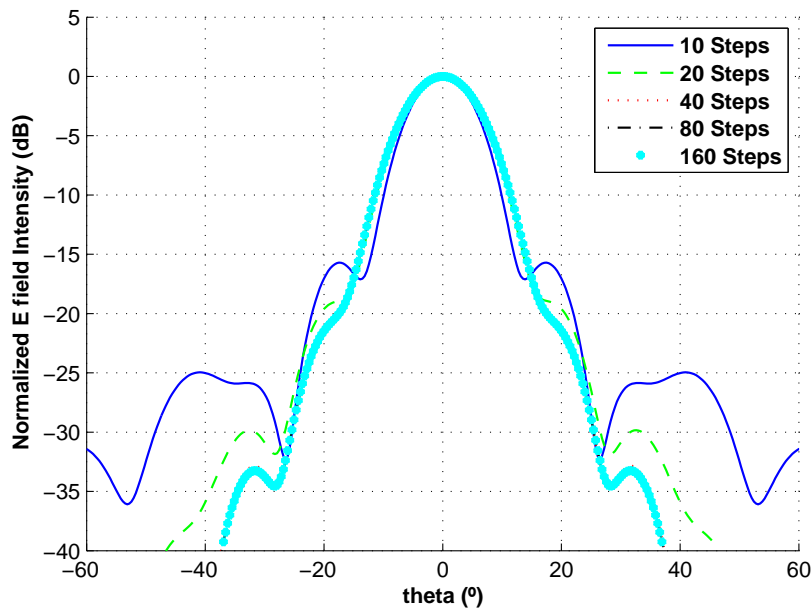


(b) H-Plane

Figure 5.11: Convergence of the radiation pattern for different number of modes at the horn aperture.

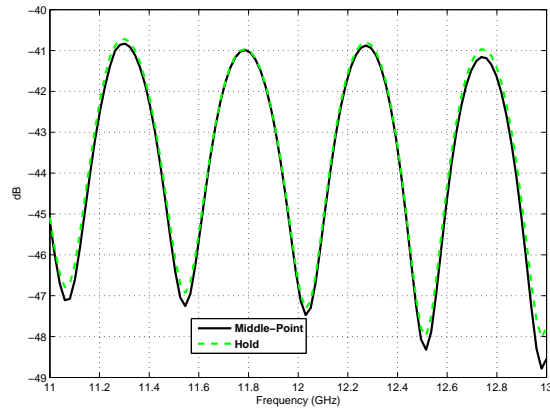


(a) E-Plane

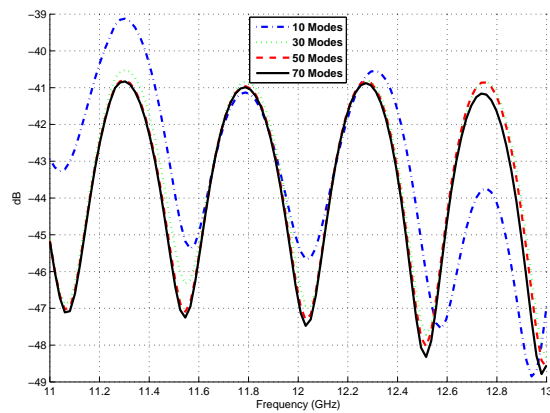


(b) H-Plane

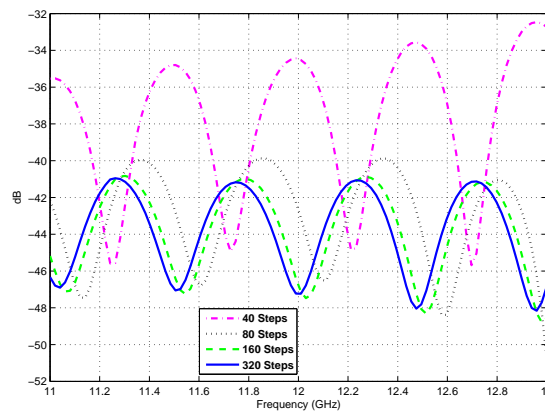
Figure 5.12: Convergence of the radiation pattern for different number of waveguide steps.



(a) For different discretization methods.



(b) For different number of modes.



(c) For different number of waveguide steps.

Figure 5.13: Convergence study of the return loses.

the radiation of complex 3D physical structures can be analyzed without the need of high computational resources, in reduced time and with accuracy for the important figures of merit.

The verification cases are summarized in the following text, showing the different types of horns that have been studied.

Tercius

- **Source:** Created in this work as a simple test case.. Simulated with CST Studio.
- **Input radius:** $5mm$.
- **Aperture radius:** $50mm$.
- **Length:** $100mm$.
- **Waveguide sections:** 10.
- **Modes at aperture:** 70.
- **Modes at input:** 7.

Hispasat 1C

- **Source:** [8]
- **Corrugated.**
- **Input radius:** $11.7mm$.
- **Aperture radius:** $58.011mm$.
- **Length:** $385.7mm$.
- **Waveguide sections:** 222.
- **Modes at aperture:** 70.
- **Modes at input:** 14.

Conical horn

- Source: [9]
- Non-corrugated.
- Input radius: $18mm$.
- Aperture radius: $70mm$.
- Length: $302.5mm$.
- Waveguide sections: 100.
- Modes at aperture: 70.
- Modes at input: 18.

High performance feed horn

- Source: [10]
- Non-corrugated.
- Multiple slope profile.
- Input radius: $0.203mm$.
- Aperture radius: $1.2mm$.
- Length: $8.771mm$.
- Waveguide sections: 300.
- Modes at aperture: 70.
- Modes at input: 11.

Chapter 6

Horn-type antenna design

6.1 Motivation

After having verified the correct behavior of all the developed code, now it is time to demonstrate its usefulness. This will be accomplished by designing some antennas. In this chapter two conical antennas will be designed (corrugated and non-corrugated) with a specified beamwidth marked by a radiated field level of $-10dB$. This is the classic example of a horn antenna used as a feed for a parabolic reflector.

6.2 Design process

The design process that has been followed is illustrated at Figure 6.1 on the next page. Each step will be briefly described here:

- Specifications: Define the desired beamwidth, the phase error, the waveguide port radius and whether the horn is corrugated or not.
- Theoretical sketch: Using graphical calculation with normalized radiation patterns get a first approximation of the aperture radius and the corresponding waveguide length for the desired phase error.
- Simulate: Using the Mode-Matching software compute the radiation pattern. If the specifications are met go ahead for the next step, if they are not satisfied tune the aperture radius (and consequently the

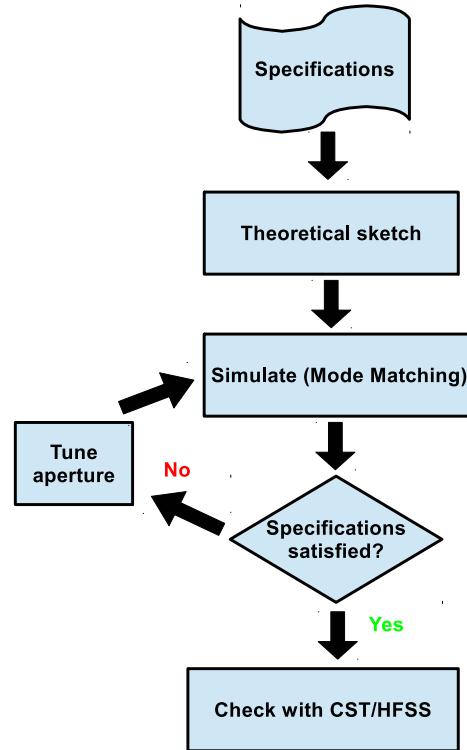


Figure 6.1: Horn design flowchart

horn length) and repeat this step. This may require several iterations before getting the desired radiation pattern.

- Check the results: The results provided by the Mode-Matching software may be checked against a simulation performed with a commercial tool like CST or HFSS.

The main advantage of employing this algorithm based on the Mode-Matching software is that each simulation is carried out in less than a minute while calculations with CST or HFSS take quite some time in comparison, so the simulate-and-tune process would be impractically long.

6.3 Non-corrugated conical horn

The specifications for this antenna are:

- Operation frequency: $10GHz$.
- E-Plane beamwidth at $-10dB$: $\Delta\theta_{-10dB,E} = 40^\circ$.
- Low phase error: $s = 0.11$ (radians normalized to 2π).
- Waveguide port radius: $a = 10mm$.

A first design approximation was obtained by means of graphical calculation using a normalized graphic [1]:

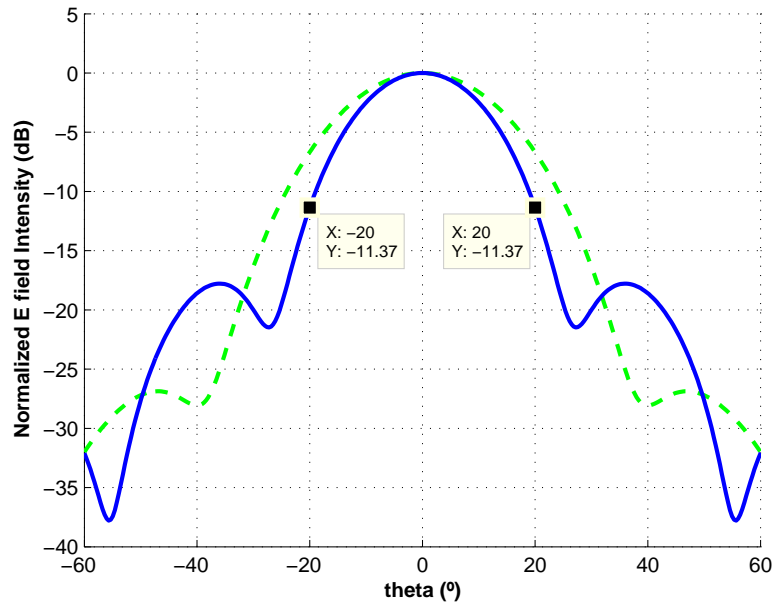
- Aperture radius: $A = 40.484399mm$
- Length: $L = 186.991302mm$

The radiation pattern obtained by this horn is shown at Figure 6.2a on the following page. It can be seen that the beamwidth is slightly narrower than desired, which means that the horn aperture should be smaller. After a couple of trials it is found that the desired beamwidth can be achieved with the following parameters:

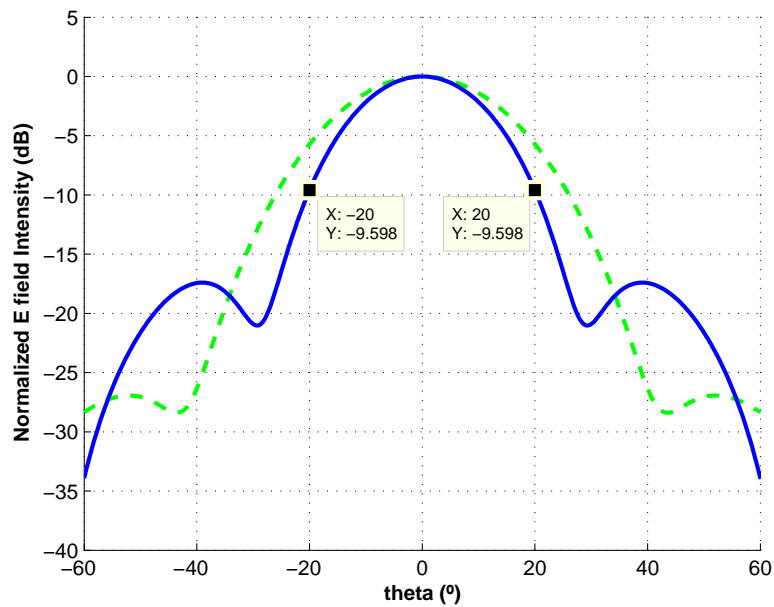
- Aperture radius: $A = 37.692372mm$
- Length: $L = 158.150177mm$

It can be seen that the radiation pattern achieved by this horn (Figure 6.2b on the next page) fulfills the specifications stated above. If this horn were going to be built, it would be a good idea to check first this design with some commercial microwave tool. This antenna has been simulated with CST Microwave Studio and the comparison between these results and the ones provided by the Mode-Matching software can be found at Figure 6.3 on page 63. It must be noted that, given our limitations in computational capabilities with respect to those required by the simulation of this antenna with CST, the mesh employed by CST may not be provide fully convergent results. This also shows the advantages of the developed analysis tool, since it can be ran with much more moderate computational resources.

A representation of the return losses of the final design for different frequency values can be found at Figure 6.4a on page 64. It can be seen that its value is around $-20dB$ for the operation frequency, which is an acceptable level.

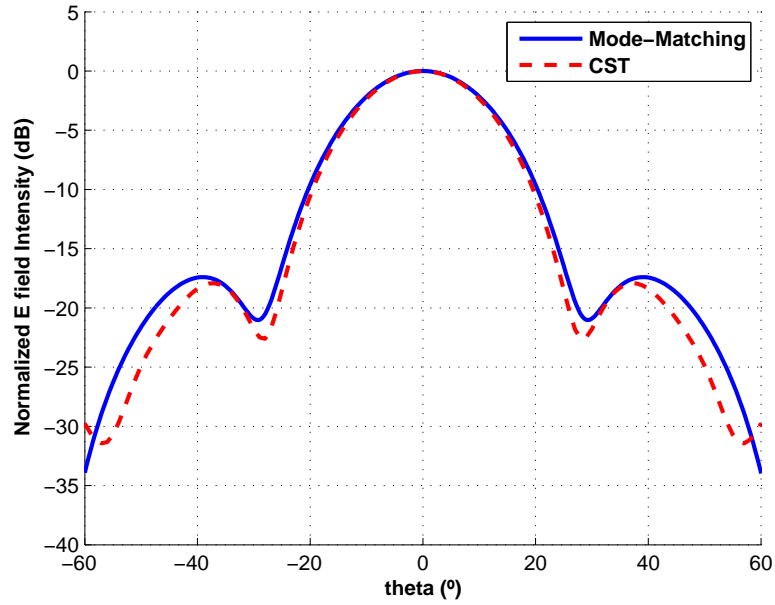


(a) Theoretical approximation

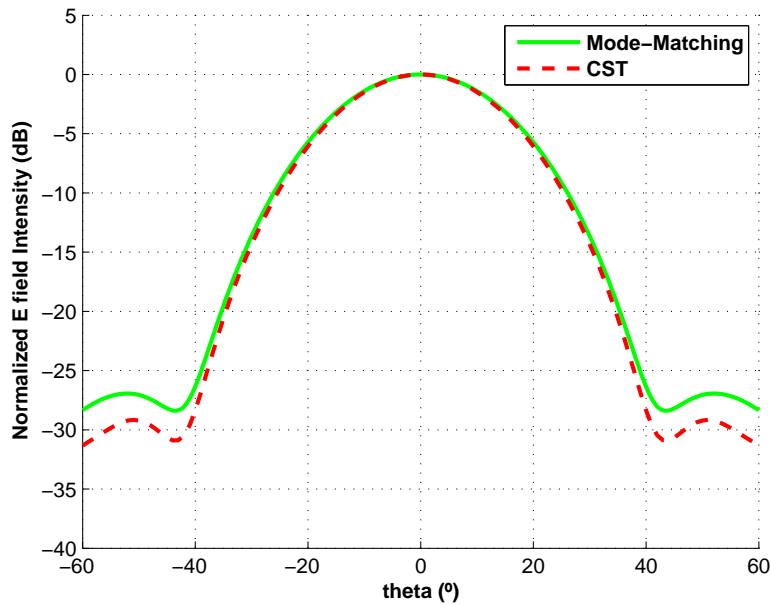


(b) Final version

Figure 6.2: Radiation pattern of the non-corrugated conical horn at $10GHz$.
E-Plane: Solid blue, H-Plane: Dashed green.

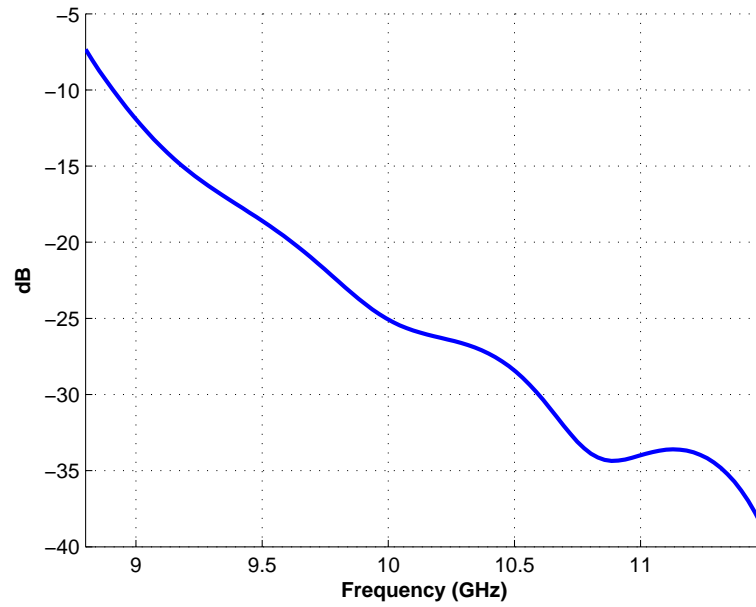


(a) E-Plane

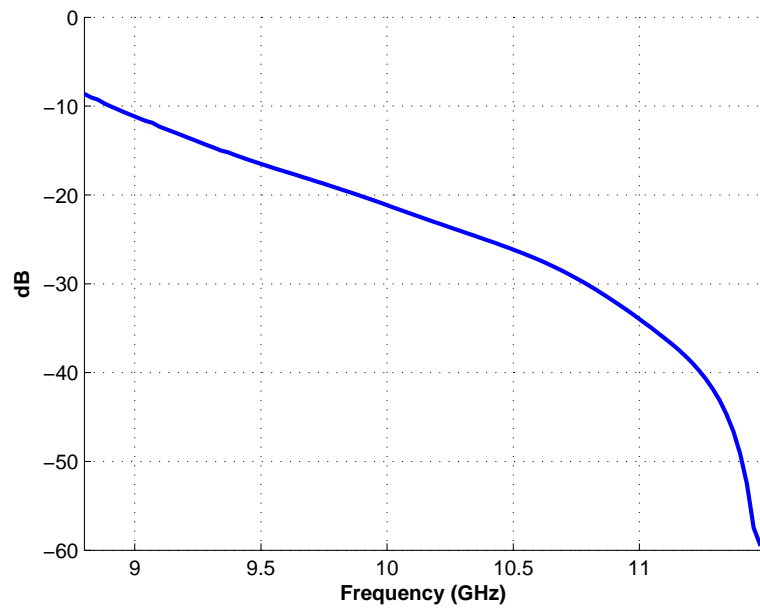


(b) H-Plane

Figure 6.3: Comparison of the results by Mode-Matching (solid) and CST Studio (dashed) at $10GHz$.



(a) Non-corrugated horn.



(b) Corrugated horn.

Figure 6.4: Return losses of the designed antennas.

6.4 Corrugated horn

The specifications for this antenna are:

- Operation frequency: $10GHz$.
- Beamwidth at $-10dB$: $\Delta\theta_{-10dB} = 40^\circ$.
- Phase error: $s = 0.20$ (radians normalized to 2π).
- Waveguide port radius: $a = 10mm$.

It is important to note that radiation pattern is (theoretically) the same for both the E-Plane and the H-Plane. This is the reason why it is not specified the plane for the beamwidth. At this point, it is also interesting to emphasize that, it will be seen in the following simulations that the radiation patterns match accurately for the main lobe but not for the secondary lobes.

A first design approximation was obtained by means of graphical calculation using a normalized graphic [1]:

- Aperture radius: $A = 55.840551mm$
- Length: $L = 213.313467mm$

Additionally it must be defined how the corrugations will be implemented. A representation of the different parameters that compose the corrugations can be found at Figure 6.5 on the following page. Ten corrugations per wavelength have been used, $t = 0.09tw$, $w = 0.91tw$ and d changing linearly from $\frac{\lambda_0}{2}$ to $\frac{\lambda_0}{4}$ (from waveguide port to aperture). This variant depth is implemented as a trade-off between return loss matching and radiation pattern. Having all the slots with $d = \frac{\lambda_0}{2}$ gives small return losses but the radiation pattern at E- and H- planes have different beamwidth. When using $d = \frac{\lambda_0}{4}$ the same radiation pattern is obtained at the two main planes at the cost of extremely high return losses. Using the variant depth permits getting the low return losses of the first case and the radiation pattern of the second.

The radiation pattern obtained by this horn is shown at Figure 6.6a on page 67. It can be seen that the beamwidth is slightly narrower than desired which means that the horn aperture should be smaller. After a couple of trials it is found that the desired beamwidth can be achieved with the following parameters:

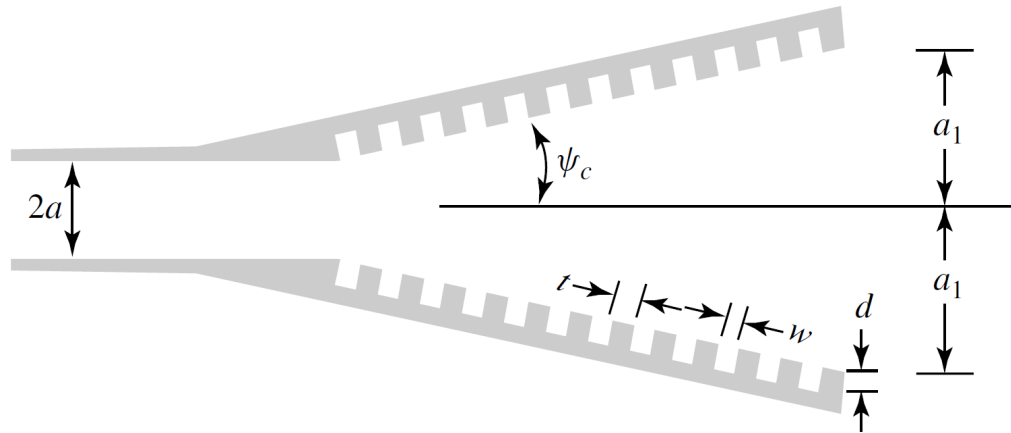


Figure 6.5: Parameters of the corrugation. Extracted from [2].

- Aperture radius: $A = 50.745100mm$
- Length: $L = 172.301185mm$

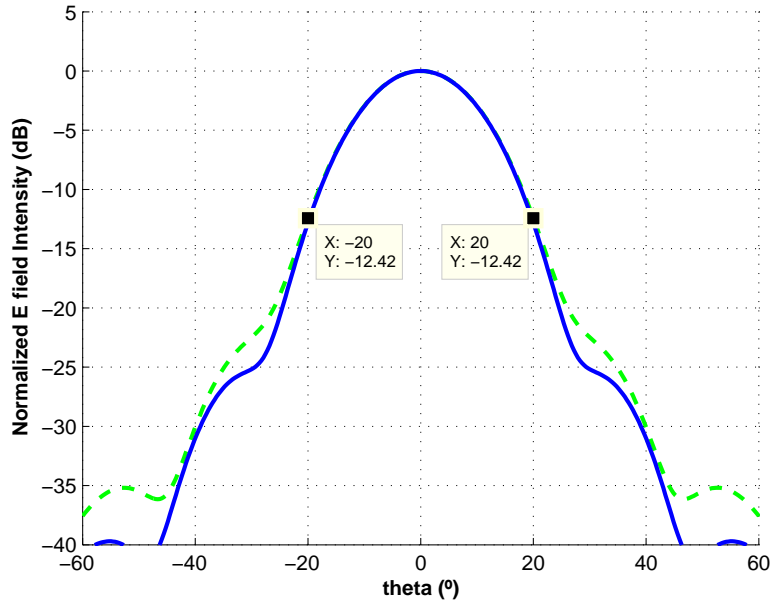
It can be seen that the radiation pattern achieved by this horn (Figure 6.6b on the facing page) fulfills the specifications stated above.

A representation of the return losses of the final design for different frequency values can be found at Figure 6.4b on page 64. It can be seen that its value is around $-20dB$ for the operation frequency, which is an acceptable level.

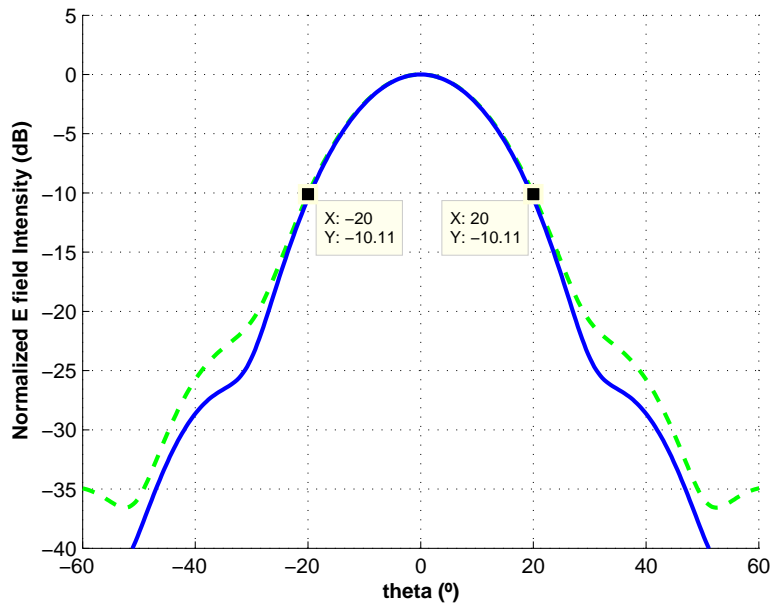
6.5 Conclusions

The main advantage of using our Mode-Matching software to design a horn antenna is that each iteration of the algorithm proposed at Figure 6.1 on page 60 takes just a few seconds while using a general purpose method would take some minutes. Therefore, if we needed to iterate ten times, the whole process could take up to almost an hour.

Since this tuning process can be tedious for the designer we have also developed a software tool that automates it.



(a) Theoretical approximation



(b) Final version

Figure 6.6: Radiation pattern of the non-corrugated conical horn at $10GHz$. E-Plane: Solid blue, H-Plane: Dashed green.

Chapter 7

Conclusions

The main goal of this work has been to develop a method for analysis and design of horn antennas that would give shorter computation times than the commercial tools. In order to improve timing we have chosen to implement the Mode-Matching method that allows us to approximate an arbitrary waveguide profile as a succession of waveguide steps.

Since horn antennas have a lot of similarities with waveguides, the study of horns requires the understanding of waveguide modes. Therefore, at the first step of this project we developed a MATLAB program that computes the electromagnetic fields inside of different waveguides and resonant waveguide cavities.

After this step, we studied the theory of the Mode-Matching method. In order to achieve a better comprehension of the method, we developed a MATLAB program that solves H-Plane rectangular waveguide problems. We proved its utility by simulating several single waveguide steps, but also a seven order bandpass filter. This last case, successfully analyzed, is a very robust validation case. It involves not only discontinuities, but cascading of GSMs (Generalized Scattering Matrices) when higher-order modes are interacting between waveguide steps.

At this point of the project we started dealing with the horns, which involved two main tasks. The first one was to convert a three dimensional real world object into a model that the Mode-Matching method could work with. For this task, different procedures have been tested. The second task was to use the data obtained by cascading the GSM inside the horn to obtain the radiation pattern of the antenna. To accomplish this we developed a program that computes the radiation integrals using the electromagnetic fields at the

horn aperture.

It must be noted that developing a fully functional and optimized Mode-Matching software would be beyond the scope of this project so for the final implementation we have used a Mode-Matching software developed by the RFCAS research group. This is the only piece of software in the project that was not completely developed in this work. The code developed in this work at chapter 3 implements the same mode-matching technique. However, the Mode-Matching code provided by RFCAS is a compiled executable file that has been optimized for speed when dealing with hundreds of discontinuities. Since the fundamentals of the Mode-Matching method were already covered in chapters 2 and 3, we believed that it was a better strategy to focus in the final problem (the horn), rather than optimizing again the initial code developed in this work in chapter 3. Nevertheless, the computation of the modal amplitudes, the radiation integrals, the discretization of the horn, the computation of the radiation diagrams, the computation of the directivity,... were fully developed in this work.

The software obtained was tested against different antenna measurements and simulation from different sources with significant success.

Once we had a functional and verified simulation tool we started the design step. Using our software we have also been able to design a couple of antennas by means of a small notebook computer.

Finally, and to demonstrate the utility of our software, we wrote a program that given the specification of a non-corrugated conical horn (beamwidth, operation frequency,...) obtains the dimensions of a horn that fulfills them. Thanks to the low execution times of the Mode-Matching method this optimization algorithm can design an antenna in less than a minute.

Future Work

Given the good results obtained by the conical horn simulator it would seem a good idea for future work to develop a pyramidal horn simulator. The process would be the same as the one followed through this work and since the radiation integrals would be done in Cartesian coordinates these calculations would indeed be easier.

Bibliography

- [1] Milligan, T. A. "Modern Antenna Design", Second Edition, John Wiley & Sons, 2005.
- [2] Balanis C. A. "Antenna Theory, Analysis and Design", Third Edition. John Wiley & Sons, 2005.
- [3] Pozar, D.M. "Microwave Engineering", Fourth Edition. John Wiley & Sons, 2012
- [4] Ruiz-Cruz, J.A. Montejo-Garai, J.R. Rebollar, J.M. "Computer Aided Design of Waveguide Devices by Mode-Matching Methods" in "Passive Microwave Components and Antennas" Published by In-Teh, 2010. ISBN 978-953-307-083-4
- [5] A. Ludwig, "Radiation pattern synthesis for circular aperture horn antennas," *Antennas and Propagation, IEEE Transactions on*, vol. 14, no. 4, pp. 434 - 440, jul 1966.
- [6] Leal Sevillano, C. A. "Análisis de bocinas mediante el método de Ajuste Modal". Personal Communication (Notes from a Master course).
- [7] Pascual García, P. "Modelos de análisis y diseño de dispositivos en guía integrada en sustrato para banda ku". Proyecto Fin de Carrera, Escuela Politécnica Superior, UAM, Sep 2012.
- [8] Jorge Teniente Vallinas, "Modern Corrugated Horns Antennas," Ph.D. dissertation, Grupo de Antenas, Departament de Ingenieria Electrica y Electronica, Universidad Publica de Navarra, 2003.
- [9] J. Reiter and F. Arndt, "Full-wave analysis of circular waveguide horn antennas including the outer wall geometry with an hybrid MM/BCMM method," in *Antennas and Propagation Society International Symposium*, 1996. AP-S. Digest, vol. 3, 21-26 1996, pp. 1984-1987 vol.3.

- [10] Tan, Boon-Kok. Leech, Jamie. Yassin, Ghassan. Kittara, Phichet. Tacon, Mike. Wangsuya, Sujint. Groppi, Christopher. "A High Performance 700 GHz Feed Horn", in *Journal of Infrared, Millimeter, and Terahertz Waves*, 2012. Springer US, vol. 33, issue. 1, pp1-5.